AN ABSTRACT OF THE THESIS OF

Heidi Ann Pattee for the degree of Doctor of Philosophy in Mechanical Engineering presented on January 23, 1992.

Title: Temperature Measurement, Electrical Characteristics, and Lorentz Mixing of Alkali Seeded Flames

Redacted for Privacy

Abstract approved: Richard B. Peterson

When trace quantities of an alkali element are added to a flame, its optical and electrical properties change significantly. Addition of alkali seed to both premixed and diffusion flames has been used in the development of two new techniques, one for flame temperature measurement and the other for enhanced mixing.

Advantage has been taken of the spectral characteristics of alkali seeds in the development of a non-invasive optical flame temperature measurement technique. The strongest resonance line of alkalis is in fact a doublet, and the two peaks can be subjected to different optical treatment. A cesium-seeded flame was exposed to radiation which was selectively filtered to yield different apparent source temperatures at the wavelengths corresponding to the doublet resonance lines. The ratio of the emission peak heights at the two wavelengths relates directly to flame temperature. This technique allows real-time measurement of flame temperatures up to 2800 K.

A second process has been investigated which takes advantage of the enhanced electrical conductivity of alkali-seeded diffusion flames. The study first required a characterization of electrical discharges through planar diffusion flames. Because of the increase in conductivity, alkali-seeded diffusion flames can carry current when a transverse electric potential is applied. The behavior of diffusion flames carrying electrical current has been investigated. The dependence on electrode position and gap is reported and the behavior is contrasted with that described in the literature for premixed flames.

A planar diffusion flame was subjected to a steady magnetic field parallel to the flow direction while an orthogonal, oscillating current passed through the flame sheet. A Lorentz body force was induced on the flame sheet which acted to move it alternately toward the fuel and oxidizer streams, improving bulk mixing in the flame. High-speed video images of the oscillating flame were analyzed to obtain its maximum lateral velocity. The results compared well with predictions from a simple theoretical model.

Temperature Measurement, Electrical Characteristics, and Lorentz Mixing of Alkali Seeded Flames

by

Heidi Ann Pattee

A THESIS

submitted to

Oregon State University

in partial fulfillment of
the requirements for the
degree of

Doctor of Philosophy

Completed January 23, 1992

Commencement June 1992

APPROVED:

Redacted for Privacy

Associate Professor of Mechanical Engineering in charge of major

Redacted for Privacy

Head of Department of Mechanical Engineering

Redacted for Privacy

Dean of Graduate School

Date thesis is presented January 23, 1992

Typed by researcher for Heidi Ann Pattee

ACKNOWLEDGEMENT

The completion of a PhD requires support, both intellectually and emotionally, from countless individuals. It is a pleasure to recognize that support and express my appreciation to those who provided it.

Dr. Richard B. Peterson has served for the past four and a half years not only as my graduate adviser, but also as a co-worker, supporter, and friend. No adviser/student relationship is entirely harmonious, and ours is no exception. We have had our differences, but have kept disagreements to a minimum and instead worked together toward common goals. At the start of this degree my skills in experimental research were minimal, and I have benefitted greatly from both the advice Rich has given and the example he has set. I feel that he has prepared me well for the career that lies ahead.

Four other faculty members have served on my graduate committee: Dr. Dwight Bushnell, Dr. Max Deinzer, Dr. A. Murty Kanury, and Dr. Jose Reyes. I appreciate the time they have invested and advice they have provided along the way. As an undergraduate assistant, Pamela Reese helped build much of the laboratory equipment. Doug Snell has provided both technical support, through numerous discussions, and emotional support as a peer and friend.

Finally, I appreciate the encouragement from my husband Dick and the many family members and friends who have stood by me throughout this time. Their contributions to this effort may be less tangible, but they are no less valued.

TABLE OF CONTENTS

LIST OF FIGURES

LIST OF FIGURES (CONTINUED)

TEMPERATURE MEASUREMENT, ELECTRICAL CHARACTERISTICS, AND LORENTZ MIXING OF ALKALI SEEDED FLAMES

1. INTRODUCTION

The simplest flame involves a chemical reaction between stoichiometrically balanced amounts of a fuel and an oxidizer. The fuel and oxidizer can be thoroughly mixed prior to reaction or they can be kept separate, coming together at their interface just prior to reacting. The former is known as a premixed flame while the latter is a diffusion flame. In either case, the character of the flame can be changed by introducing other substances into the primary reactants. The additive can be an excess amount of one of the reactants (in the case of premixed flames), an inert diluent not participating in the reaction, or a small concentration of another material which is mixed with the reactants for the sole purpose of changing some property. A substance which is added in trace concentrations for this purpose is referred to as seed material.

Depending on the material being used, adding seed to a flame can cause many changes. In the work reported here, two such effects are important. The presence of seed material, in this case an element from Group IA of the periodic table, affects both the spectral and electrical characteristics of a flame. The changes in the flame's spectral characteristics are exploited for measuring its temperature. Advantage is taken of the improved electrical properties as part of a method which enhances reactant mixing in a diffusion flame.

When a free atom undergoes a transition from one energy state to another it emits or absorbs energy at a specific frequency (or wavelength). The frequency depends on the energy levels of the two discrete states, and is unique to the particular atom. The alkali elements, those in Group IA of the periodic table, have particularly strong spectra because they are configured with a single electron in the outermost shell. The relative strength of emission is directly related to temperature. When added in even trace concentration to a flame, alkalis produce strong emission lines. Several optical methods of determining flame temperature are based on monitoring these lines.

All of the alkalis except lithium share the attribute that their strongest emission line is in fact split into a doublet. This characteristic doublet can be exploited for temperature measurement because the two peaks, although originally very similar, can be subjected to different optical treatment due to their slightly different wavelengths. The development of a flame temperature measurement technique which makes use of this concept is the subject of Chapter 4.

The addition of an alkali also changes the electrical properties of a gas. Again, the lone outer shell electron of the alkali atom is responsible for the drastic changes observed when seed is added to a flame. The most notable property change is in the electrical conductivity. Adding a small amount of an alkali to a hot gas can increase its conductivity by two orders of magnitude or more. This makes the seeded gas sufficiently conductive to carry moderate current at normal flame temperatures. To raise the conductivity of an unseeded gas to comparable levels, the temperature would have to be much higher than the limit

of many materials. Seeded flames can carry current in much the same way as a copper wire does; this is the basis of many experimental techniques.

The behavior of a conductive flame is not as simple or predictable as that of a copper wire. Studies of premixed flames augmented with electrical discharges have shown that the effects of geometry can be very important. Additionally, because conductivity is a strong function of temperature, self heating due to the current flow affects the gas properties. This in turn changes the amount of current until a balance is reached. The interactions between these effects are complex and have not previously been reported for diffusion flames. Chapter 5 is therefore dedicated to characterizing electrical discharges through seeded diffusion flames.

Body forces can be induced in a current-carrying conductor such as a copper wire by placing it in an appropriately oriented magnetic field. If the electrical conductivity of a gas is sufficiently high, it can be subjected to induced body forces in the same manner. The direction of these body forces can be controlled and they can be used to manipulate a flame. Specifically, parallel streams of fuel and oxidizer can be subjected to an oscillating force which will improve the mixing at the interface. Investigations of this method for enhanced mixing of a seeded diffusion flame are described in Chapter 6.

2. BACKGROUND

2.1 General

Flames are frequently altered by adding trace quantities of a material which does not directly participate in the primary combustion reaction. This process, known as "seeding" the flame, is done for various reasons. In general, the motivation involves using the presence of the seed to change one or more properties of the flame. A seed will generally be present only in trace amounts, but if it is evenly distributed throughout the reaction zone it can profoundly influence the flame's properties. Newman and Page (1973) have demonstrated the importance of uniform distribution of seed material in flames.

Elements from Group IA of the periodic table are commonly used as seed material in flames. This group, usually referred to as the alkali elements, includes sodium, potassium, and cesium. All alkali elements are configured with a single electron in the outermost shell. The ability of an alkali seed to affect a flame's physical properties can usually be attributed to this characteristic. Most of these changes are a direct result of the fact that alkalis ionize very readily.

An alkali seed affects a flame in many ways. For example, addition of alkali metals has been shown to suppress the formation of soot in premixed flat flames (Haynes et al., 1978). Place and Weinberg (1965) have experimented with seeded counterflow diffusion flames, and reported that both the quantity and size of carbon particles could be controlled. Another purpose of alkali seeds in flames is as chemical flame suppressants (Mitani and Niioka, 1984). When the mist of an alkali salt is added to a premixed flame, there is a critical concentration above which

the flame is extinguished. In fact, alkali metal salts have been used as flame suppressants for more than 100 years, although the exact mechanism of their operation is not thoroughly understood.

The two most important properties of alkali seeds are their unique optical and electrical properties. Alkali metals exhibit strong emission at characteristic resonance lines corresponding to their electronic transitions (Gaydon, 1974). The strength of these emission lines is directly related to temperature, and this relationship has been used in the development of temperature measurement techniques (Gaydon and Wolfhard, 1970; Strong and Bundy, 1954a, 1954b, 1954c). Due to the low ionization potential of alkalis, their presence in a flame can raise its electrical conductivity two orders of magnitude or more (Angrist, 1982). The enhanced conductivity allows a current to be passed through the flame; this concept has many applications, including power generation and augmentation of the heat output of combustion sources (Davies, 1965). The optical and electrical enhancement of alkali seeded flames are each discussed below.

2.2 Optical Temperature Measurement of Flames

Combustion researchers often need a quick, reliable, inexpensive means of measuring flame temperatures. Thermocouples are simple and popular temperature measurement devices which convert heat energy to electrical energy (Malmstadt et al., 1981). Pt/Pt-Rh thermocouples are frequently used for temperature probing of cool flames. Thermocouples must be corrected for radiative and conductive losses as well as for catalytic effects, but they provide a simple and consistent means of determining flame temperature profiles (Gaydon and Wolfhard, 1970). The

major disadvantage of using thermocouples to probe small flames is that their presence disturbs the flame. At temperatures above about 2000 K, thermocouple probing is frequently impractical because of platinum's melting point. It is necessary to use tungsten thermocouples, which are incompatible with an oxidizing environment. Sheathing for an inert gas purge severely reduces spatial resolution and increases the flow disturbance.

Optical, laser based methods have the advantage of probing a flame without disturbing it and have been used extensively in optically clean environments. One accurate laser technique, CARS (Coherent Anti-Stokes Raman Spectroscopy), has been useful in soot-laden environments and in highly luminous flames (Lapp and Hartley, 1976). However, the specialized equipment required is not readily available in many research labs. There are several simpler optical techniques which can be implemented with common laboratory equipment. The most popular of these, the line reversal method, measures flame temperature by equating the emission to that of a radiation source whose temperature is adjustable and calibrated.

Kurlbaum (1902a, 1902b) described a simple method of measuring flame temperature by comparing the spectral brightness to that of a known, continuous radiation source. Radiation from the source is passed through the flame. If the flame temperature is lower than that of the source, the characteristic resonance lines appear in absorption against the constant background; if the flame is at a higher temperature than the source, the resonance lines appear in emission. The techniques Kurlbaum developed were later applied to the specific resonance lines of sodium, and the name "line reversal" was adopted. Other alkalis have

also been used effectively (Klingenberg and Mach, 1976). The line reversal method, described in detail in many places (Gaydon and Wolfhard, 1970; Penner, 1949; Reif et al., 1973), became popular during the middle of this century. To implement the method, the temperature of the source is varied until the resonance lines appear neither in absorption nor in emission. The flame temperature and the source temperature are then assumed to be equal. The source temperature can be measured, and the flame temperature is thus inferred.

The emission intensity of a blackbody is a function of both temperature and wavelength, as described by Planck and approximated by Wien's law (Siegel and Howell, 1981):

$$I \propto \lambda^{-5} e^{-\frac{c}{\lambda T}} \tag{2.1}$$

For a specific wavelength, the emission intensity of a source at a given temperature can be equated to that of a blackbody radiator at a somewhat lower temperature (known as the "brightness temperature" of the source). When radiation is passed through a gas or flame, some of it will be absorbed at the specific wavelengths corresponding to ground state transitions of species present. Additionally, the gas emits radiation at these wavelengths based on its own temperature. Application of Kirchoff's law (Siegel and Howell, 1981) yields a differential equation describing the resultant radiation intensity:

$$dI = (I_f - I) \alpha \, dx \tag{2.2}$$

In general, both α and I_f can vary with position. If only emission in a very narrow wavelength band (e.g. that corresponding to a spectral line)

is considered, and if the gas composition and temperature are constant, the value of α can be taken as constant in an element of gas. The solution of equation (2.2) is then:

$$I e^{\alpha x} = \int I_f \alpha e^{\alpha x} dx \tag{2.3}$$

Equation (2.3) can now be solved for the flame geometry. Integrating across the flame (from $x = 0$ to $x = l$) and applying the boundary condition $I(x = 0) = I_b$:

$$I = I_f(1 - e^{-\alpha l}) + I_b e^{-\alpha l} \tag{2.4}$$

The difference between intensity at the spectral line wavelength and that at a nearby wavelength can now be determined. For the latter, $\alpha = 0$ and the intensity is simply I_b. The difference ΔI, which represents the height of an emission or absorption peak above the background, is:

$$\Delta I = (I_f - I_b)(1 - e^{-\alpha l}) \tag{2.5}$$

In traditional line reversal, the temperature of the background radiation source is adjusted until $\Delta I = 0$. Solving equation (2.5), $I_b = I_f$ for this condition, meaning that the background temperature equals the flame temperature ($T_b = T_f$). Since the temperature of the background source has been calibrated, the flame temperature is thus determined.

Line reversal has been used in many laboratory flame studies on both premixed and diffusion flames (Wolfhard and Parker, 1949). It is useful for fundamental studies but has also been implemented for practical temperature measurements in a variety of applications including, for example, an MHD generator (Daily and Kruger, 1976) and rifle muzzle

flash (Klingenberg and Mach, 1976). Thomas (1968a) has shown that the technique can be adjusted for use in flames containing particles and in cases where boundary layer effects are present. Due to its simplicity, versatility, and low cost, the method has become widely used and well-accepted (Gaydon and Wolfhard, 1970).

Line reversal can be modified to eliminate the need to balance a background source. Thomas (1968b) developed a method which instead used two different background temperatures and compared the intensity difference ΔI obtained for each. He derived an expression which directly relates the ratio of the two values to flame temperature:

$$R = \frac{\Delta I_1}{\Delta I_2} = \frac{I_f - I_{b1}}{I_f - I_{b2}} \tag{2.6}$$

Expressing the intensities as in equation (2.1):

$$R = \frac{e^{-\left(\frac{c}{\lambda T_f}\right)} - e^{-\left(\frac{c}{\lambda T_{b1}}\right)}}{e^{-\left(\frac{c}{\lambda T_f}\right)} - e^{-\left(\frac{c}{\lambda T_{b2}}\right)}} \tag{2.7}$$

From equation (2.7), measurement of the peak height at each of two background temperatures can be used to deduce flame temperature. The peak is not "reversed" (or balanced) at all during the process. Since the source need not be adjusted to match the flame, temperatures several hundred degrees Kelvin above the maximum attainable background temperature can also be measured. The disadvantage of this two-temperature method is that the source must continually be switched between T_{b1} and T_{b2}. Because of the time lag, there is no assurance that the same flame temperature is being measured with each source.

In addition to their strong resonance lines all of the alkali elements except lithium share the characteristic that their strongest emission line is actually a doublet. The reason for the doublet (Kuhn, 1969) is that an elevated outer electron can reside in two states with different spin direction, or spin quantum number. The wavelengths of the doublets for alkali elements are shown in Table 2.1. For sodium the wavelength separation between the two peaks of the doublet is less than one nanometer, so at low resolution the peaks appear as a single line. As the molecular weight of the alkali increases so does its peak separation, with the cesium doublet being separated by about 42 nm (Weast, 1973). This characteristic doublet can be exploited for temperature measurement because the radiation at the two wavelengths, although very similar in origin and intensity, can be subjected to different optical treatment.

Table 2.1 Wavelengths of Alkali Doublets

Element	Doublet Wavelengths (nm)	Separation (nm)
Sodium	588.995 589.592	0.597
Potassium	766.491 769.898	3.407
Rubidium	780.023 794.760	14.737
Cesium	852.110 894.350	42.420

2.3 Electrical Discharges through Seeded Flames

The temperature of a flame can be raised by inputting energy in the form of an electrical discharge. The resistive heating (or "Joule heating") augments the enthalpy of the flame. The main difficulty lies in

attempting to distribute the electrical energy evenly through the flame gases. Because electrical conductivity increases rapidly with temperature, the discharge tends to confine itself to a narrow channel. The enthalpy of the discharge channel is then quite large relative to that of the surrounding gas. Weinberg (1986) describes a simple demonstration of this effect. When two electrodes are placed across a premixed flame, the discharge initially chooses a path just downstream of the flame surface. The channel then drifts downstream at the gas velocity, preferring to take a longer path because the conductivity has been greatly increased due to self-heating. Only after the channel becomes greatly elongated does the arc strike back to follow the flame surface again. Because of this strong tendency for discharges to channel, other means of spreading them throughout a larger region are required for uniform heating.

Karlovitz (1962) proposed using a highly turbulent flame as a means of distributing a discharge evenly. Reactants were seeded with an alkali element to raise gas conductivity to the necessary level. He mentioned the possibility of using diffusion flames, but carried out his experiments on premixed natural gas/air flames. In the ten years that followed, the nature of high-voltage discharges in premixed flames was a topic of substantial interest. Fells et al. (1967) reported extensively on d.c. discharges in premixed propane/air flames, characterizing the effects of seed concentration, electrode gap, electrode material, and gas flowrate. Lapp and Rich (1963) performed similar studies on acetylene/air flames, concentrating on the voltage/current characteristic curves and conductivity measurements. The results of these premixed

flame studies will be discussed in further detail in Chapter 5, where they are compared and contrasted with the present investigation of diffusion flames.

There were many apparent discrepancies among early published results. These were resolved by Ulherr and Walsh (1971), who identified two distinct modes of discharge which exhibit quite different behavior. They categorized the results of earlier authors and studied the conditions under which the transition between the modes occurs. They described the two modes as follows. Mode A was characterized by low current and a relatively diffuse discharge. The anode exhibited "many tiny arc spots which flick around the surface." The second mode, which they called mode B, was a higher current discharge occupying a smaller volume of the flame. A large, bright, steady glowing region was observed on the anode.

Planar diffusion flames differ fundamentally from premixed ones in their ability to carry current because the reaction and hot product zone (and hence the highly conductive region through which the current travels) occupies a much smaller volume. It is generally more difficult to disperse a discharge uniformly without developing filamentary "arcs" through the flame. Most of the published work that deals with diffusion flames subjected to electric fields is quite different in its focus than that reported for premixed flames. Several authors (Place and Weinberg, 1965; Katz and Hung, 1990) have reported the use of electric fields to control particle formation in flat, counterflow diffusion flames. These flames were unseeded, however, and carried very low currents relative to

seeded flames. Nakamura (1959) investigated the effect of an electric field on emission spectra from a flat co-flowing diffusion flame, but again the flame was unseeded and apparently carried little current.

2.4 Magnetic Field Effects

It has been known since the early work of Lorentz that a current carrying conductor placed in a magnetic field will experience a force perpendicular to both the current direction and the magnetic field lines (see e.g. Halliday and Resnick, 1967). This force can be induced in any conductor, whether it is a copper wire or a current carrying region of an ionized gas. Lorentz forces can therefore be used to accelerate a gas, provided that it carries a current in the presence of a properly oriented magnetic field.

Much of the past research on conductive gases subjected to magnetic fields has related to magnetohydrodynamic (MHD) power generation (Angrist, 1982). A hot gas is seeded with either potassium or cesium and forced through a rectangular duct. When a perpendicular magnetic field is imposed an electric potential is produced across the duct. An external circuit can be connected for power generation. The current which flows through the gas also interacts with the magnetic field, resulting in a Lorentz force which opposes the gas flow and causes a deceleration (or pressure drop). Conversely, if power is supplied rather than extracted the Lorentz force will act instead to accelerate the gas. This process has been proposed for constructing a hypersonic flow facility to produce gas velocities far in excess of those attainable in flow tunnels based on combustion stagnation sources or arc jet facilities (Crawford et al., 1990).

The possibility of using a magnetic field to spread the discharge through a flame for more uniform heating has been considered. Kimura and Ogiwara (1974) used a magnetic field to create a swirling discharge which in turn tended to promote turbulence in the premixed gases. Chen et al. (1965) described a rotating discharge through which a premixed flame passed. This resulted in a less filamentary, more evenly distributed discharge. From the reference frame of the moving gases, the discharge appeared as a spiral. There is a maximum rotation rate which still guarantees a well-distributed discharge. Weinberg (1986) reasoned that an even distribution of heat could also be achieved by an arc channel that is not perfectly permeable.

Using the same concept with a different orientation of the magnetic field, a Lorentz force can be induced perpendicular to the direction of gas flow. Dimmock and Kineyko (1963) reported experiments in which forces of this type were used to deflect premixed flames. Their experiments used both a.c. and d.c. currents. They proposed applying the concept to rocket exhaust streams as a method of altering the thrust vector. A transverse Lorentz force of this type can also be used to oscillate the interface between parallel streams of fuel and oxidizer to promote mixing. One long term application of such a technique would be a rapid forced mixing of reactants for high-speed propulsion systems such as that envisioned for use in SCRAMJET engines (Bussing and Eberhardt, 1989).

3. EXPERIMENTAL APPARATUS

3.1 Gas Delivery and Seeding

All of the studies described in the following chapters require a precisely controlled supply of seeded reactant gases. Figure 3.1 shows the system used for supplying fuel and oxidizer for the experiments. Bottled gases are used, their pressures being controlled with Matheson Model 8 two-stage pressure regulators. Gas flowrates are monitored using Matheson 600 Series 150 mm tube rotameters equipped with high-accuracy needle valves. Pressures are measured with a dial gauge at the rotameter exit.

The fuel (CH_4 or H_2) is sent into a mist chamber for seeding with a CsCl solution. The mist chamber is shown schematically in Figure 3.2. The mist chamber was made from a SounDesign Model 1822 ultrasonic humidifier which was modified for these experiments. To modify the humidifier, the fan which normally circulates room air was removed. Instead, the body of the humidifier was fitted with a two-way valve which connects to both the fuel line and an inert (N_2) purge line. The liquid reservoir tank was removed and the size of the liquid chamber inside the humidifier was reduced to hold only about 200 ml of the solution to be atomized. For the experiments described here, the liquid in the chamber was usually CsCl solution ranging in concentration between 0.2 and 0.5 M. An ultrasonic transducer beneath the liquid surface generates a fine mist, which is carried along with the fuel stream toward the burner. The rate of seeding is adjustable with a slide switch on the unit. At the gas flowrates used in these experiments, the CsCl solution was introduced at a rate which gave approximately 0.04 to 0.1 mole percent

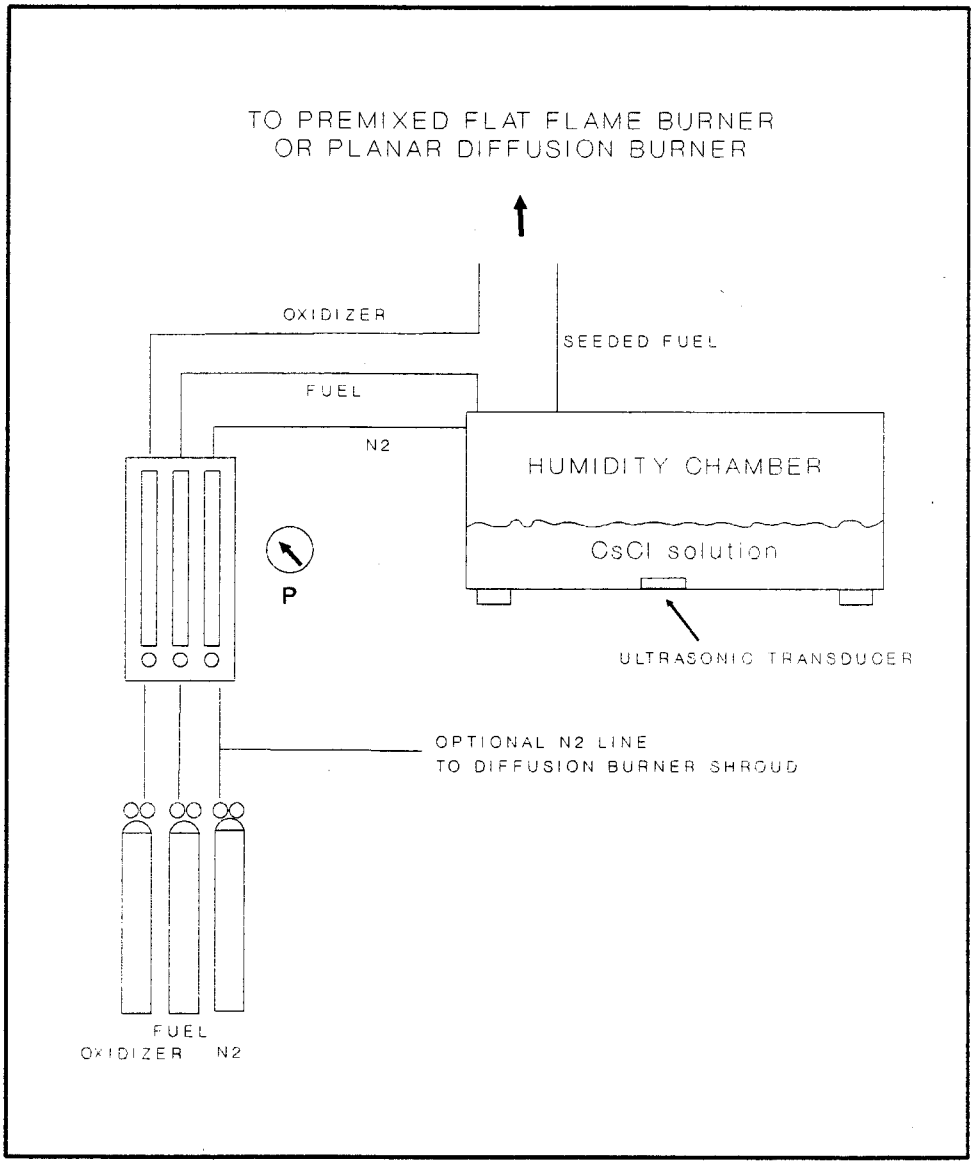

Figure 3.1 Reactant Gas Delivery System

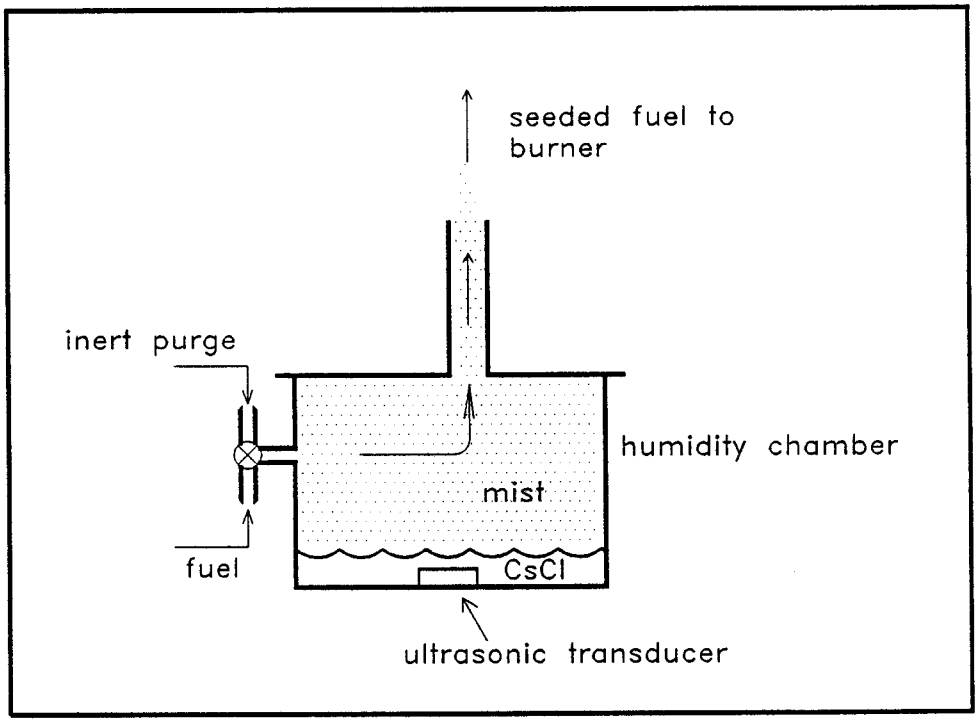

Figure 3.2 Humidifier Chamber for Introducing Seed to Fuel

in the gas stream. The entire mist chamber was sealed with silicone caulk to prevent leakage of any combustible mixture into the laboratory. The top of the chamber was modified to accommodate either of two different burners at the gas exit. The two burners, one for examining premixed flames and the other for diffusion flames, are described in Section 3.2.

The entire mist chamber/burner assembly was mounted on an x-z stage. In general, probing of different flame regions was accomplished by translating the assembly relative to a fixed measurement system. A vernier scale on the stage allowed both vertical and horizontal positioning to within 0.1 mm.

3.2 Burners

Two different burners have been used in the research described here. Each has distinct features which make it useful for certain types of work. For the temperature measurement experiments described in Chapter 4 a premixed flat flame burner was used. In premixed flames the fuel and oxidizer have been thoroughly combined prior to the reaction occurring. The reaction rate is thus controlled by kinetics, since the fuel and oxidizer are in intimate contact and available to react with one another. Flat flames are a special class of premixed flames in which the radial velocity profile of the gases entering the flame has been rendered essentially constant. As a result the flame's temperature and species profiles are not highly dependent on the radial flame position, but rather depend primarily on distance in the flow direction. Flat flames are sometimes referred to as "one-dimensional flames" for

this reason, since the spatial position in only one dimension is critical for property measurement. In practical burners the velocity profile cannot be made perfectly flat, but conditions approaching the ideal can readily be achieved. Flat flame burners are useful for examination of flame profiles and verification of new techniques because one additional constraint on the measurements has been removed.

For the premixed flat flames described in Chapter 4, a stainless steel screen burner similar to that described by Altenkirch et al. (1979) was used. As shown in Figure 3.3, the premixed reactants enter the bottom of the burner and go through a series of screens to smooth the flow. The burner body, screens, and spacers are made of stainless steel to lessen the corrosive effects of the salt solution used for seeding. The spacing and mesh sizes of the smoothing screens can be changed to optimize flow characteristics for different flames. The top screen, above which the flame is stabilized, can be cooled by flowing water through 0.3 mm hypodermic tubing which is woven through the screen. The burner diameter is 43 mm, but can be reduced to 20 mm for exploring high speed flames without increasing the working range of gas flowrates. A 30 mesh stainless steel screen can be positioned about 17 mm above the burner to help stabilize the flames.

The experiments described in Chapters 5 and 6 deal with diffusion flames rather than premixed ones. In a diffusion flame the fuel and oxidizer are not mixed together, but kept separate. The two separate gas streams are then brought together and react at their interface. In diffusion flames the rate of reaction is controlled by the diffusion rate of the reactants into the flame. Once the fuel and oxidizer have come together in the correct proportions to react, the chemical rate is

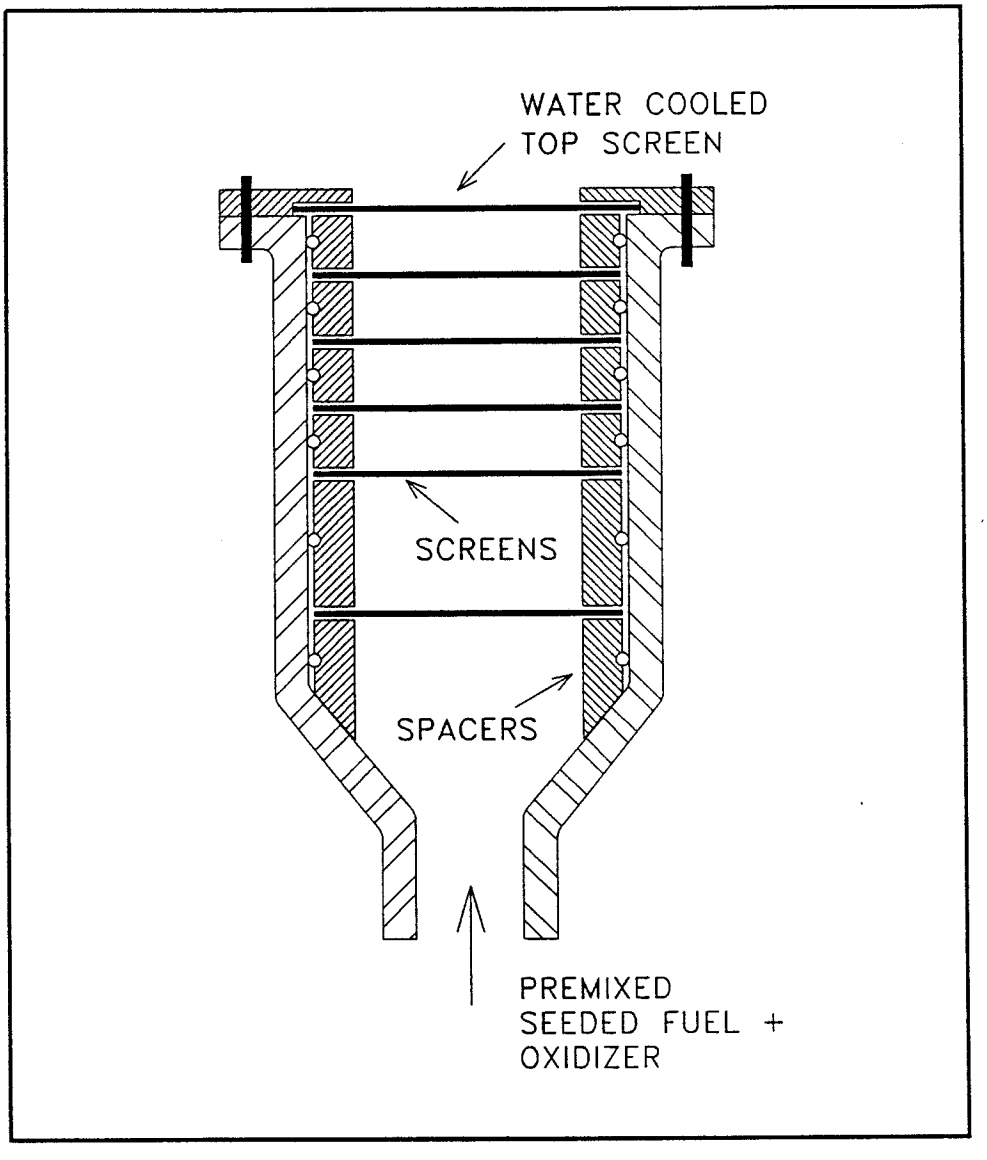

Figure 3.3 Premixed Flat Flame Burner

considered infinitely fast. A diffusion burner is therefore used to model an entirely different class of problems than those represented by premixed flame studies, and its construction is quite different from that of a premixed burner.

Just as there are numerous designs of premixed burners, only one of which has been used here (the flat flame burner), there are also numerous designs of diffusion burners. The fuel and oxidizer can be co-flowing or counter-flowing. One reactant can surround the other (e.g. flow through concentric tubes), resulting in a cylindrical reaction zone, or the reactants can meet at a single plane. For the work described here, a co-flowing planar diffusion flame was used.

Figure 3.4 details the planar diffusion burner used in the present study. Parallel streams of fuel and oxidizer issue from long, narrow slots with equal velocity in a burner of the type originally described by Wolfhard and Parker (1949). A shroud of inert gas surrounds the reactants to stabilize the flame and prevent interaction with room air.

The burner was fabricated from three 0.1 cm thick panels, each measuring 2.5 cm by 7.5 cm. The panels were made of fused quartz because they must be electrical insulators while still withstanding extremely high temperatures. The parallel panels connect to stainless steel end plates which serve as the slot ends as well as connection points for the electrode holders, which are further discussed in Section 3.4. This configuration results in burner slots which measure 2.3 cm in length by 0.5 cm wide. A 3 cm by 5 cm rectangular chimney (omitted from Figure 3.4 for clarity) contains an inert nitrogen shroud for 25 cm past the

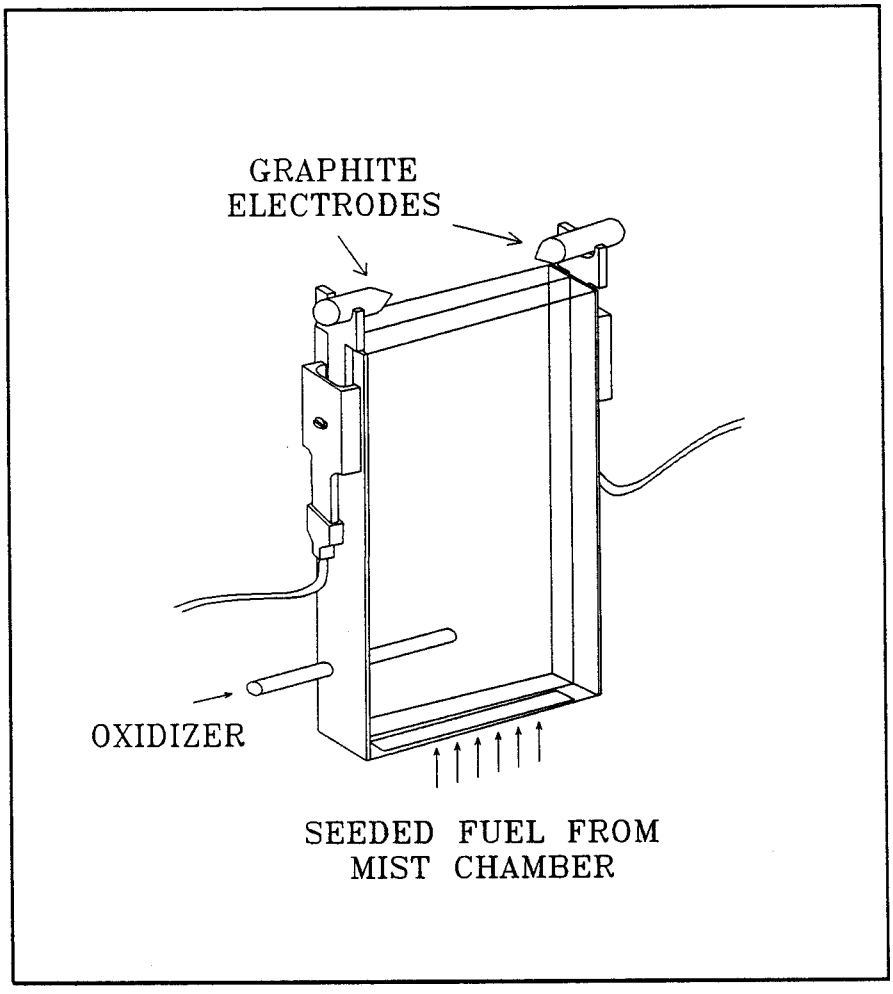

Figure 3.4 Co-flowing Planar Diffusion Burner

exit plane, well beyond the region of interest in the flame. The chimney is fitted with quartz observation windows on all four sides in the region near the flame.

3.3 Thermocouple Measurements and Corrections

In Chapter 4, a new optical temperature measurement method for flames is presented. As with any new technique, verification using an accepted procedure is critical. To validate the temperature profiles obtained using the new method, conventional thermocouple probing was also used on the same flames. Although thermocouple probing of flames has several drawbacks, it has been widely used and is an established technique.

Simply stated, a thermocouple is a device used to convert a temperature into an electrical signal. It consists of two dissimilar metal wires joined at one end. A voltage develops across the open leads which is directly related to the temperature of the junction. The main problems of using a thermocouple for flame work can be broken into two groups. First, the presence of the thermocouple, no matter how small, disrupts the flow field somewhat. This is particularly bothersome if very sharp temperature gradients must be resolved. The second category of problems are due to the fact that the thermocouple is not at the same temperature as the flame. Radiative and conductive losses from the bead result in its equilibrium temperature being lower than that of the flame, sometimes by several hundred degrees K. Corrections are possible but depend on knowledge of the material properties of the thermocouple.

For the study described in Chapter 4 a "Type B" (Pt-30% Rh / Pt-6% Rh) thermocouple was used. This type was chosen because its maximum temperature is about 2000 K, the highest available for a thermocouple which is compatible with an oxidizing environment. A 0.25 mm wire (approximately 0.60 mm bead) was selected as being small enough for good spatial resolution yet large enough to be fairly robust. The thermocouple wires were sheathed in a 15 cm long double-hole ceramic tube to within about 3 cm of the bead. The sheath tube was firmly clamped in position and the burner was moved to obtain temperature profiles. A Keithley Model 740 Scanning Thermometer was used to convert the voltage signal to temperature. It has a single log mode which was used to take 100 temperature measurements at a rate of one each 500 ms. Both the range and average of the 100 readings were automatically calculated.

For a flat flame, conduction to the lead wires will not be an issue if the flame diameter is sufficiently large. Because the flat flame has a nearly constant velocity profile, the heat flux down the wires will be small. For small flames, however, this term becomes important. For the premixed flat flames studied here, it was necessary to correct the thermocouple measurements for both radiative and conductive losses.

The steady state temperature of the thermocouple bead represents a balance of the radiative, conductive, and convective effects. At steady state,

$$\dot{Q}_{conv} + \dot{Q}_{rad} + \dot{Q}_{cond} = 0 \qquad (3.1)$$

The first two terms can be approximated for the bead, and this is the approach normally taken (Fristrom and Westenberg, 1965). This yields an expression for the radiative loss term, which is used as a correction to the measured temperature value:

$$\Delta T_{rad} = \frac{\epsilon \sigma d_{bead}}{2k} (T_{tc}^4 - T_{\infty}^4) \tag{3.2}$$

To consider the conduction losses as well, however, the problem is more complex. The thermocouple wire and bead were modeled numerically to examine the relative effect of the conductive losses in small diameter flat flames. The temperature profile was assumed to be perfectly flat, and all temperatures outside the flame were taken as ambient. This is a reasonable model for a flat premixed flame. The thermocouple bead was located at the center of the flame. Figure 3.5 shows the results of numerous calculations, obtained by gradually increasing the flame diameter. When actual temperature profiles are taken, the flame diameter is not changing but rather the length of lead wire which resides within the flame. For a flame at 2000 K, the conduction losses are significant when measurements are made less than about 1 cm from the flame edge (corresponding to a 2 cm diameter flame in the model).

The greatest uncertainty in the thermocouple corrections is in the emissivity of the bead surface used in calculating the radiative loss term. The magnitude of the radiative correction term is on the order of 300 K, so this uncertainty is considerable. For the types of flames measured here the uncertainty in the final temperature is approximately 80 K.

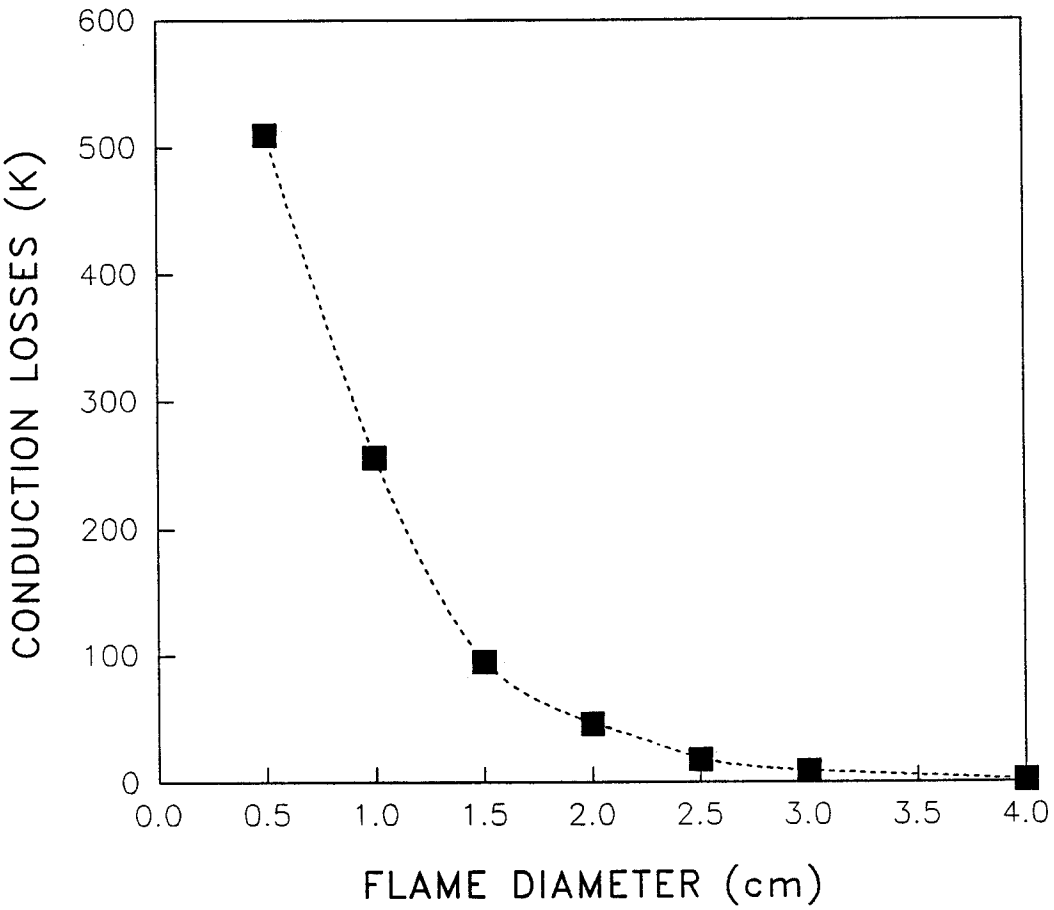

Figure 3.5 Thermocouple Conduction Losses for Small Diameter Flat Flames

3.4 Electric and Magnetic Fields

The diffusion flame work described in Chapters 5 and 6 required subjecting the flame sheet to properly oriented electric and magnetic fields. The characterizations in Chapter 5 were carried out using a d.c. electric field. The work discussed in Chapter 6 used an a.c. electric field and a steady magnetic field.

The d.c. electric field for the property characterization was generated by passing the output of a 280 V Variac through a rectifier and filter circuit. Output from a 60 V/80 A full-wave bridge rectifier was filtered using two 4200 μF/200 V Sprague Powerlytic capacitors, in series with one another but in parallel with the rectifier output. The resulting d.c. voltage had a maximum ripple factor of 0.5%. For the a.c. electric fields the rectifier/filter circuit was bypassed.

The voltage was applied across graphite electrodes situated at either end of the diffusion burner slots. The position of the electrodes can be seen in the diffusion burner diagram (Figure 3.4). The electrodes are 6 mm diameter graphite rods which are pointed to 45° cones at their ends. They are held stationary in the clamps attached to the burner endplates. Set screws allow both the gap between the electrodes and their height above the exit plane of the burner to be varied for parametric studies. The electrodes were rapidly consumed during the experiments and had to be replaced frequently to maintain the desired gap.

A 10 Ω (for d.c. studies) or 50 Ω (for a.c. studies) power resistor was wired in series with the electrode gap for two purposes. First, it prevented the possibility of a short circuit, which would blow

the Variac's 8 A fuse. Second, it could be used indirectly for current measurements. The applied voltage across the electrodes was measured directly with a Tektronix DM502A autoranging digital multimeter. Flame current was inferred by measuring the voltage drop across the power resistor with a second DM502A digital multimeter.

To produce the forces necessary for the enhanced mixing described in Chapter 6, a steady magnetic field was established with proper orientation relative to the gas flow. A magnetic flux density of up to 0.035 T (350 gauss) was generated by an external coil such that the **B** lines ran parallel to the gas flow. The configuration of the electric and magnetic fields relative to the burner is shown in Figure 3.6. The magnet was fabricated from approximately 900 turns of 20 gauge magnet wire wound around a hollow 7 cm i.d. aluminum core over a length of 5.5 cm. The total resistance of the magnet is 7.5 Ω. For the voltages used here up to 500 W of heat energy was dissipated by the electromagnet, so care had to be taken to prevent overheating. The flame region of interest was about 1 cm above the top of the magnet, and the flux density there was lower than that within the central core. The characteristics of the magnet were measured using a UGS3503 ratiometric linear Hall effect sensor, and the results are shown in Figure 3.7. The flux density is quite linear with applied voltage. Voltage for the magnet came from the rectified and filtered output of a 150 V Variac. The rectifier/filter were the same as those used for generating the d.c. electric fields in the property characterization experiments.

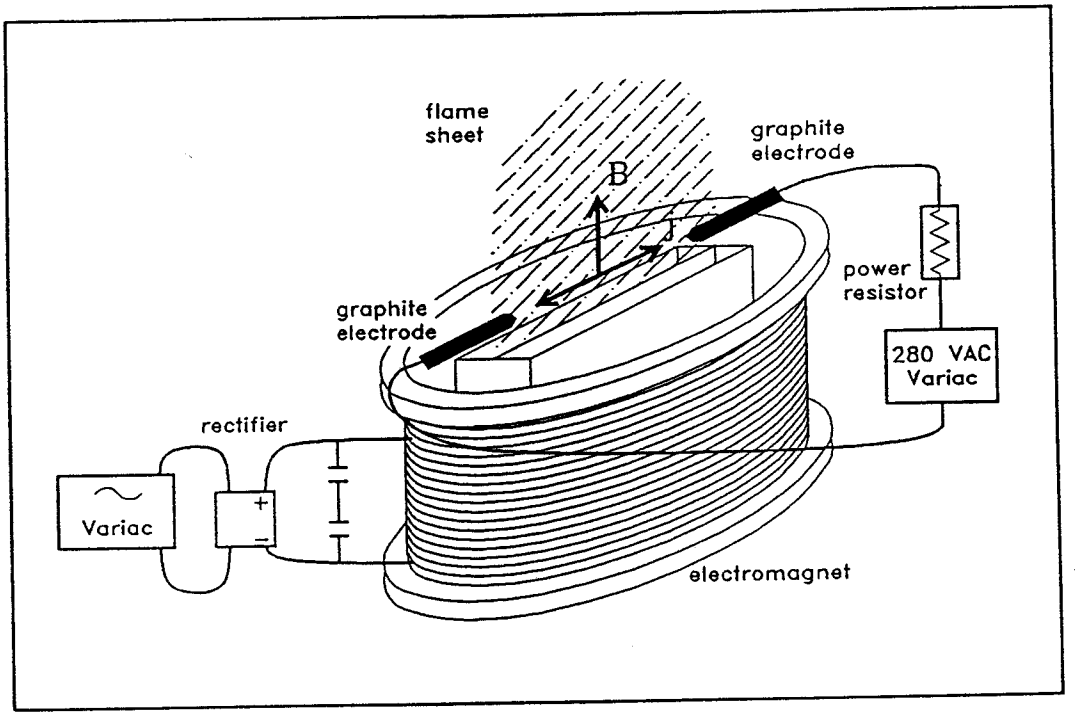

Figure 3.6 Electric and Magnetic Fields

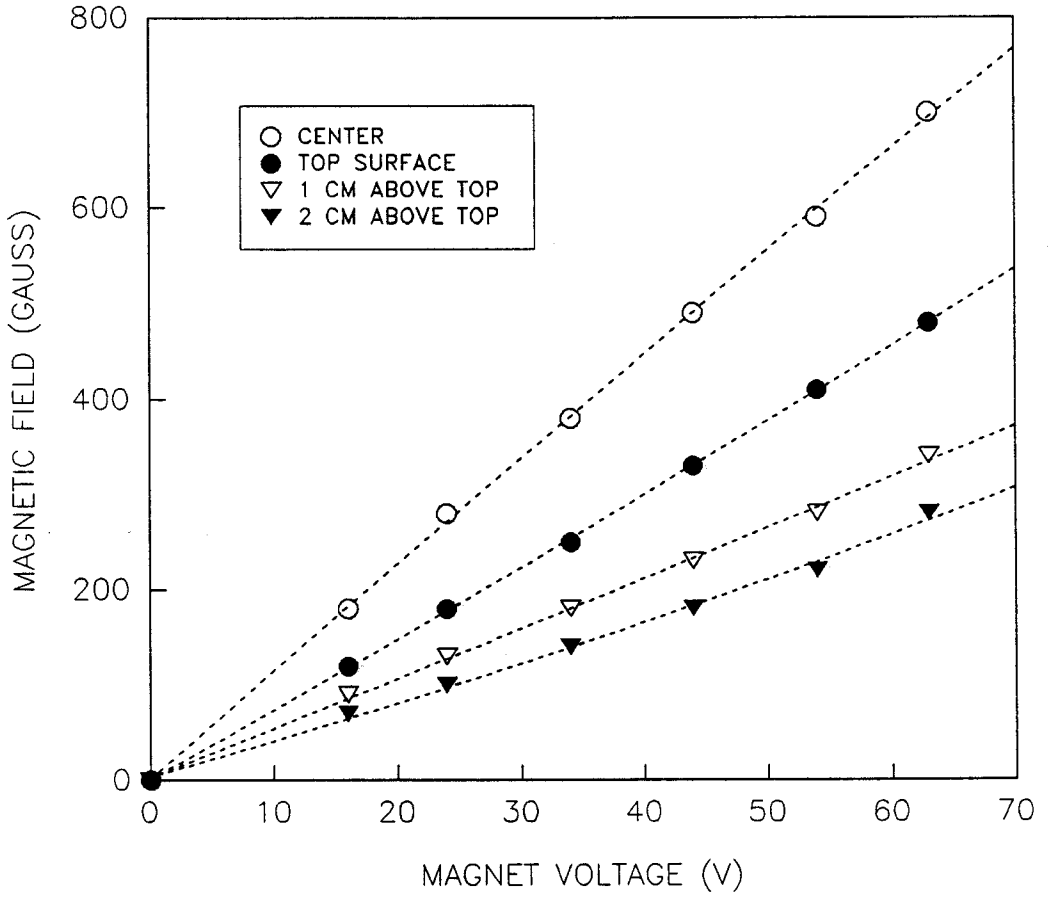

Figure 3.7 Magnetic Flux Density as a Function of Voltage and Position

3.5 Optical System

Figure 3.8 shows the optical system used for the temperature measurements described in Chapter 4. Its primary components are a background radiation source, a temperature-reducing color filter, focusing lenses, an aperture, and a spectrograph equipped with a photodiode array detector. The detector interfaces with a computerized data acquisition system, which will be described separately in Section 3.6.

A 500 W/120 V Sylvania EHD double coil tungsten/halogen lamp with a quartz envelope served as the background radiation source. It was powered with the output from a 150 V Variac. Normal operating voltages for the lamp ranged from 60 to 120 V. The operating temperature of the lamp was calibrated to determine filament temperature versus applied voltage. This was accomplished by performing a series of power measurements using various known filters placed between the lamp and a calorimeter. By considering the emissive properties of the tungsten filament (De Vos, 1954) and the transmission characteristics of the lamp's quartz envelope, the filters, and the measuring device, filament temperatures were inferred as follows.

For a specific lamp voltage setting, an Scientech Model 38-0101 volume absorbing disc calorimeter and Scientech Model 37-2002 power and energy meter were used to measure transmitted power through each of three color filters. The three filters used were an OG590, an RG695, and an RG850. For each filter, a ratio of the filtered power to the unfiltered value was calculated. Because the geometry remained constant, the power ratio was independent of the solid angle being measured.

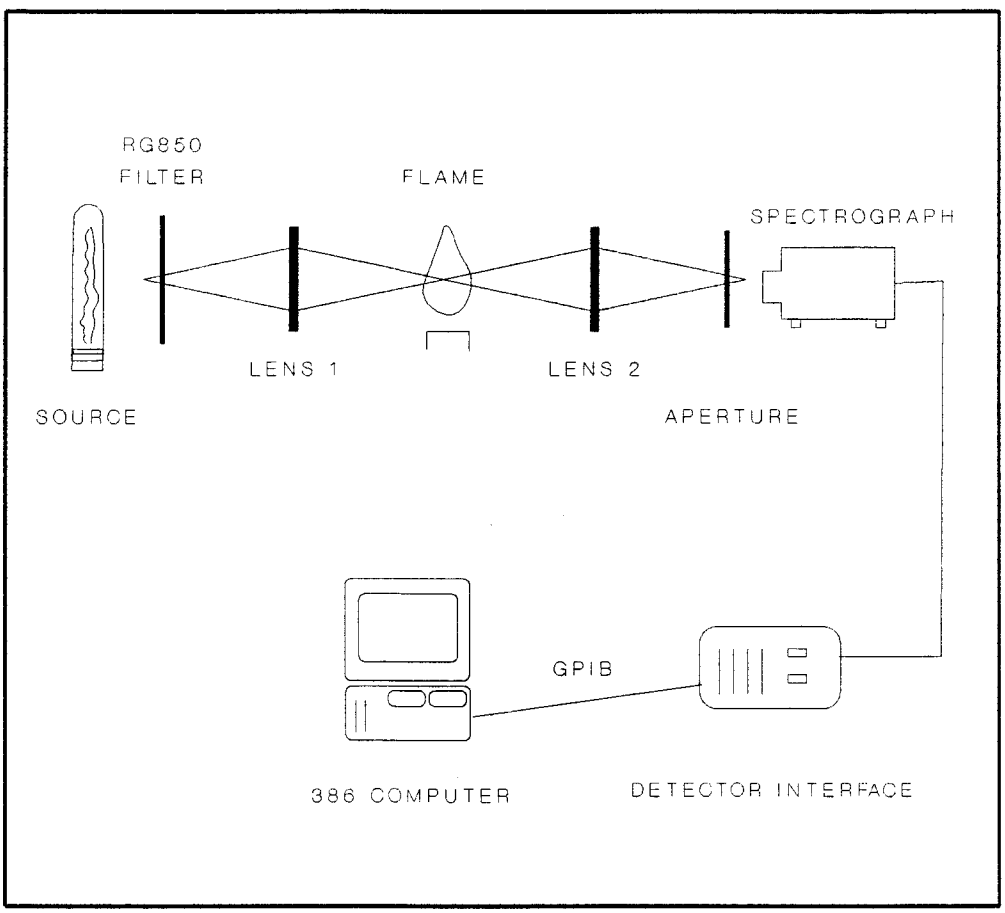

Figure 3.8 Optical System

The expected power ratio for a given filament temperature can also be determined analytically. Assuming a true filament temperature, and knowing the filament's emissivity characteristics at that temperature, the total power emitted over all wavelengths can be calculated from theory. If the intensity at each wavelength is multiplied by the known transmittance of a color filter, a somewhat lower power emission results. Both values can be corrected to account for the transmission characteristics of the quartz lamp envelope and the absorber disc. The ratio of these two values is characteristic of the temperature and the filter. This procedure was applied repeatedly for a series of temperatures and the three color filters, and a plot of power ratio versus temperature was prepared for each filter. These curves are shown in Figure 3.9. For each filter, the power ratio reaches a flat maximum; in general, these maxima occur at lower temperatures as the filter cut-on wavelength increases.

To calibrate the lamp, data were taken at seven lamp voltages. For each, the power ratios for the three filters were converted to temperature using the theoretical curves described above. If the experimentally obtained ratio fell in the flat region of the curve for one filter, only the curves of the other two filters were used to estimate temperature. Good agreement among the three filters was achieved. Figure 3.10 shows a calibration curve of filament temperature as a function of lamp voltage. Error bars are shown to represent 95% confidence intervals, based on the spread in experimentally obtained temperature values at each voltage. From theoretical considerations, the equilibrium filament temperature would be expected to vary approximately as the square root of voltage. The rate of energy input is proportional to

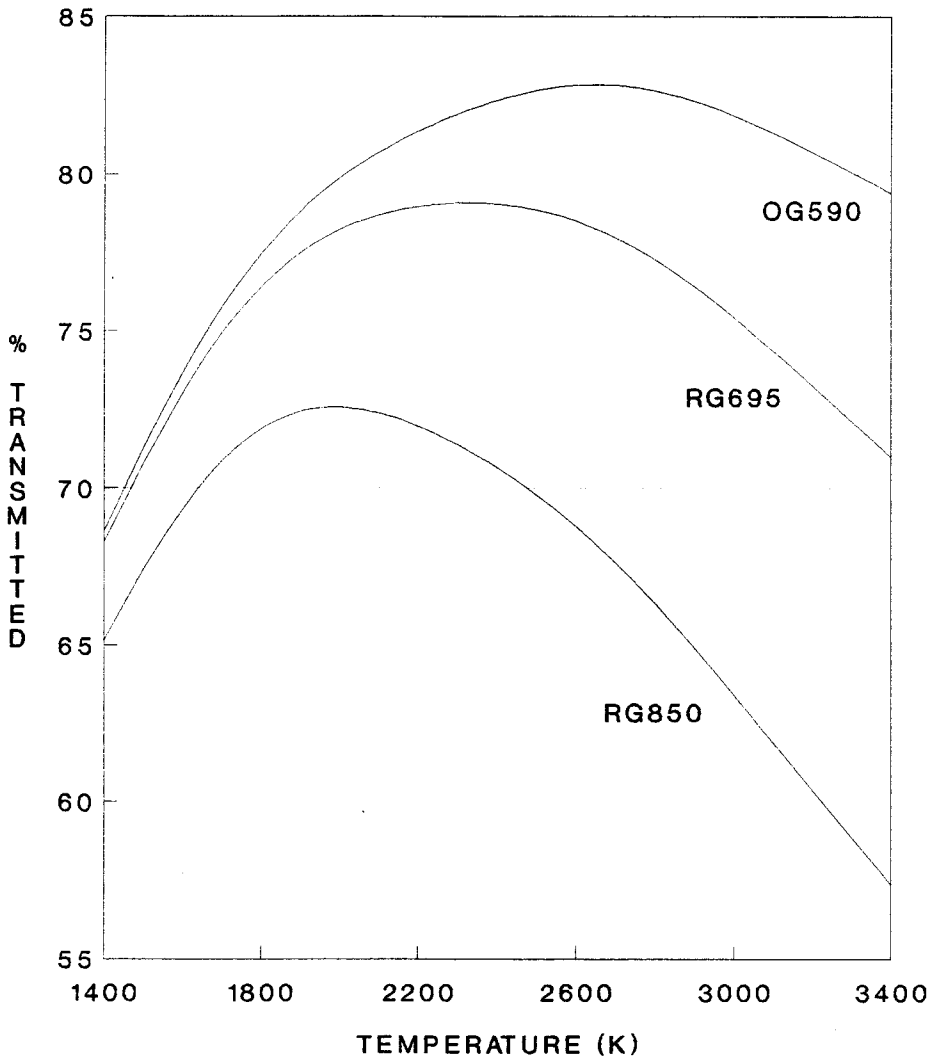

Figure 3.9 Color Filter Transmission as a Function of Temperature

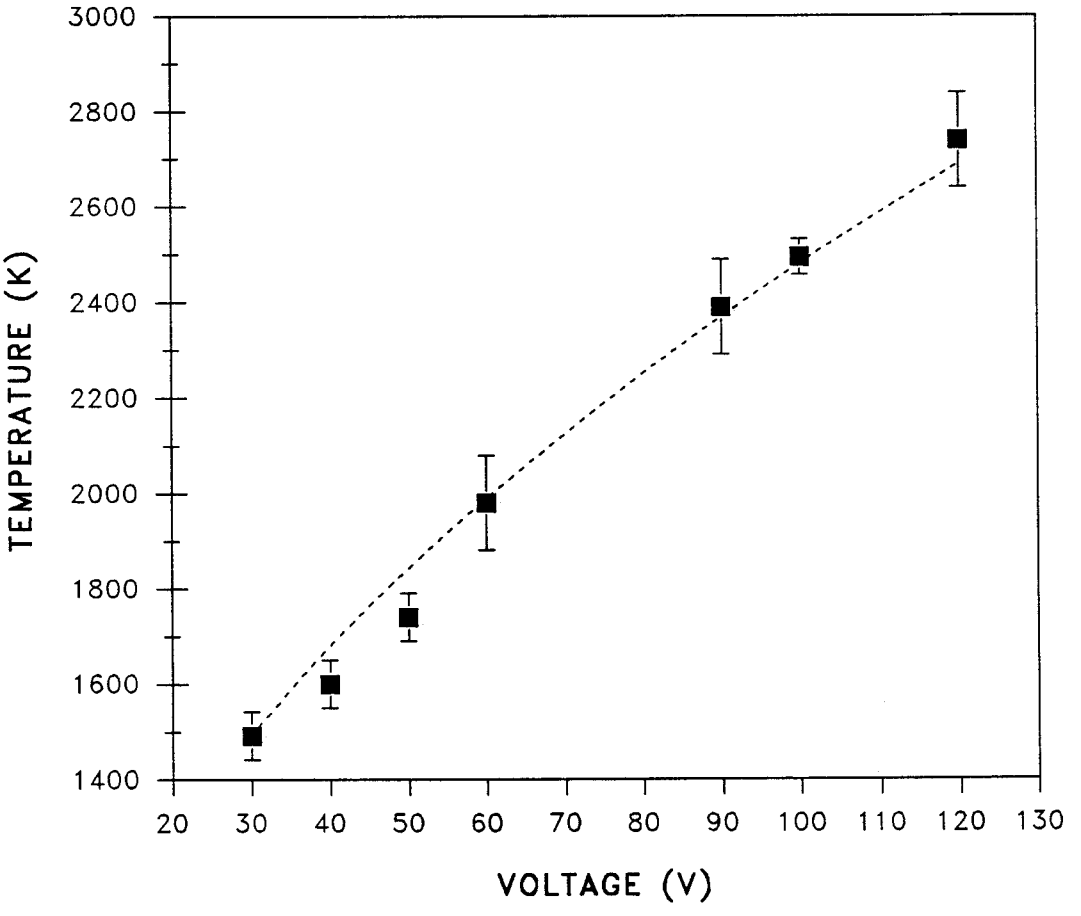

Figure 3.10 Tungsten Lamp Calibration Curve

voltage squared, while the primary mode of energy loss is by radiation and is proportional to the filament temperature to the fourth power. The dotted line in Figure 3.10 is a regression line of T against $V^{1/2}$, and the experimentally obtained data follow the predicted relationship with a correlation coefficient of 0.992.

Radiation from the lamp was passed through an RG850 color filter with a nominal cut-on wavelength of 850 nm and a transmittance of 0.91 above 900 nm. This filter was specifically chosen because its cut-on corresponds closely to the resonance doublet of cesium, a necessary condition for applying the temperature measurements described in Chapter 4. At the transition wavelengths of cesium, 852 and 894 nm, the filter transmittances were 0.55 and 0.88, respectively.

After passing through the color filter, radiation from the lamp was focused into the flame, then refocused onto the slit of a spectrograph. A pair of 10 cm focal length, 2.5 cm diameter coated double convex lenses were used. Spacing and alignment were maintained by mounting all optical components on an optical bench either permanently or with holders having magnetic bases. An adjustable iris served as a field stop and limited the intensity reaching the spectrograph.

A high-resolution spectrograph (Instruments SA Model HR320) was used to generate the emission spectra. The fixed spectrograph slit was oriented vertically and had a width of 0.05 mm. The slit was also modified (blocked off) to a total height of only about 0.1 mm. A holographically ruled diffraction grating with 600 grooves/mm gave a spectral resolution of 0.125 nm/element. An EGG/PARC Model 1455 512-element photodiode array detector with a Model 1462 detector controller was used. It had a scan range of 64 nm; this was compatible

with the 42 nm wavelength spacing of the peaks being monitored. An EGG/PARC Model 1461 optical multichannel analyzer/detector interface scanned the pixels serially with a total scan time of 0.015 ms for the 512 element array.

The detector sensitivity decreased profoundly at higher wavelengths, an effect which had to be considered in calculating peak ratios. The higher wavelength cesium doublet at 894 nm fell just at the edge of the detector's useable range and was marginally measurable. The sensitivity at 894 nm was about 1/15 that at 852 nm, which severely hampered the ability to accurately measure small emission or absorption peaks at the higher wavelength. The sensitivity ratio was calculated by taking numerous scans of a known, approximately gray radiation source and comparing the measured intensity ratio to that calculated from theory.

3.6 Data Acquisition

A computerized data acquisition system was used to accumulate and analyze the spectrograph output. A National Instruments GPIB interface connected the detector with a Zenith Z-386 personal computer equipped with a high resolution color monitor. The EGG/PARC applications software for the detector interface was used during setup, for taking initial measurements, and during alignment of the optical train. For actual measurements, however, it was necessary to do time averaging of the spectra to improve the signal to noise ratio. Both the nature of the flames (which were not completely steady) and the low detector sensitivity at high wavelengths contributed to the high noise level in

individual scans. The pre-written software package did not have the capability to do the necessary time averaging, so another approach was taken.

A complete interfacing routine for the detector (included as Appendix B) was written using the ASYST data acquisition programming language. A short ASYST algorithm for establishing minimal communications was provided by EGG/PARC. This program was expanded to allow a variety of data acquisition modes as well as nearly real-time graphic output. The menu-driven program allows direct communication with the detector interface for setting basic parameters and querying the detector's status. The user can also input ASYST commands directly to perform non-standard file or data handling activities.

During more routine activities involving the spectrograph, scans can be taken with or without time averaging over a variable number of scans; an optional background scan can be subtracted; and scan data can be permanently saved for later use. The temperature measurement technique described in Chapter 4 is also incorporated into the program. The user can obtain peak ratios for the two cesium peaks, or can have the program use this information to calculate the flame temperature using a numerical root-finding algorithm. If a hardcopy of a saved scan is desired, it can be imported as an ASCII file into one of several plotting software packages.

3.7 Experimental Procedures

Before lighting the burner, the mist chamber was purged with N_2 for at least three minutes. This ensured that a combustible mixture could not be present within the chamber before the start of an experiment.

The two-way valve was then switched to direct fuel into the chamber. Repeated attempts were made to establish a small diffusion flame at the burner outlet. Eventually the fuel concentration inside the chamber would be high enough for a flame to be established. Regardless of which burner was installed above the mist chamber, a diffusion flame was always established at the start of the experiment.

When the flat flame burner was in use, oxidizer was gradually mixed with the fuel before it entered the bottom of the burner. As the fuel/oxidizer ratio was decreased, the cone-shaped flame began to flatten. Eventually a flat disk-shaped flame sat just above the top burner screen. If the oxidizer was further increased, the flame anchored to the screen and the screen glowed red. With further increase in the flow of oxidizer the flame would sometimes flash back through the screen into the burner body. Care had to be taken to prevent this situation. For flames which were flat at mixtures very near the stoichiometric fuel/oxidizer ratio it was possible to pass the maximum flame speed without flashback occurring. The flame then once again began to take on a cone shape, just as it did when it was fuel-rich. When air was used as the oxidizer, heating of the top screen was not usually a concern. With hotter oxygen flames, however, the top screen needed to be cooled by running cold water through the tiny hypodermic tubing "heat exchanger" woven through the screen.

When the diffusion burner was used, the oxidizer stream was gradually introduced until the velocities of the two reactant streams were matched. Flowrates were adjusted to approximately 20 cm^3/s for each reactant. A N_2 shroud flow was then established around the reactant streams to ensure that the only flame present was the planar one at the

fuel/oxidizer interface. Depending on the experiments being performed, the chimney could be placed around the burner to contain the N_2 flow and further smooth the flame.

Once the desired flame was established the ultrasonic transducer was activated, generating a mist of CsCl which entered the burner along with the gas stream. In the diffusion flame studies, the voltage across the electrodes was gradually increased until a current path through the flame was established. Once the conduction path had been initiated and the graphite electrodes heated up the voltage could be decreased. In experiments requiring a magnetic field the voltage across the electromagnet was gradually increased during an experiment, which lasted about 30 seconds.

3.8 Image Analysis

For the experiments described in Chapter 6, high speed video recordings of the flames were needed. To record the effects of the Lorentz force a Kodak high-speed video camera was used to capture images of the flame while the magnetic field was increased to its maximum value. The camera was capable of recording up to 1000 frames/s, but at very fast speeds it was difficult to light the area sufficiently to provide good images. In these studies rates of both 250 and 500 frames/s were used successfully; analyses were done on the images recorded at 500 frames/s.

The recordings were replayed at either 30 frames/s or "jogged" at 1 to 4 frames/s. The former represents a playback nearly 17 times slower than the original experiment and was useful for confirming the existence

of the predicted behavior. The 4 frame/s "jog" rate was used when individual frames were to be analyzed. Segments of the videos being replayed at both rates were transferred onto conventional VHS format for later viewing and analysis.

Individual frames of the video footage were also analyzed quantitatively. A Data Translation frame grabber, interfaced with an Apple Macintosh IIci, was used to digitize successive frames for which the experimental conditions were known. Each frame was then individually examined using Image Analyst software on the Macintosh. A variety of measurements could be performed on the images, including automatic differentiation of areas with different gray scale values. This feature was useful for measurements on the flames, which were very bright against a dark background. A "caliper" tool on the screen was calibrated based on the known dimensions of the electromagnet. It was then used to measure lateral distances moved by the flame between successive frames.

Individual images could also be saved to disk, but each image file required over 300 KB of storage space. When a hardcopy of an image was desired, it was saved as a TIFF file and transferred to a DOS formatted disk. The TIFF file was then viewed on a NeXT workstation using the Icon program. From within this program, hardcopy printout with a laser printer was possible.

4. REAL-TIME TEMPERATURE MEASUREMENT OF SEEDED FLAMES

4.1 Introduction

This chapter describes an adaptation of the conventional line reversal technique which has been developed to provide direct measurement of flame temperature without the need to balance the emission of a background source. The new method also overcomes the primary disadvantage involved in using two different background source temperatures (Thomas, 1968b), which is the lack of time resolution. It can be used to probe flames up to 2800 K. This method was primarily developed for temperature characterization of highly luminous, seeded H_2/O_2 diffusion flames which are being subjected to electric and magnetic fields (this study is discussed in greater detail in Chapter 6). The technique is well suited for this purpose since the flames already contain atoms of a Group IA element, a necessary condition for implementing line reversal. The method has been tested using premixed flat flames which are useful for evaluating a new method because temperature variation in one spatial dimension has been removed. Cool flames were probed using the new technique so that Pt/Pt-Rh thermocouple measurements could be used for verification.

4.2 Theoretical Development

Group IA elements such as sodium, potassium, and cesium share the characteristic of having two strong, closely spaced emission lines. Both lines can be monitored simultaneously, and will reverse at the same background brightness temperature. It is also possible to expose the two transitions to different effective source brightness temperatures.

If a filter with a cut-on wavelength between the two transitions is placed in front of the source, the background intensity at the lower wavelength will be reduced more than that at the higher wavelength. This effectively causes the two emission peaks to respond as if each were being measured against a different comparison source. For sodium, the emission doublet is too closely spaced for practical implementation of this technique. Potassium, rubidium, and cesium, however, are all potential candidates for this method. Equation 2.7 is modified to reflect the difference in wavelength, with the wavelength dependent terms no longer canceling as they did previously:

$$R = \left(\frac{\lambda_2}{\lambda_1}\right)^5 \left[\frac{e^{-\left(\frac{c}{\lambda_1 T_f}\right)} - e^{-\left(\frac{c}{\lambda_1 T_{b1}}\right)}}{e^{-\left(\frac{c}{\lambda_2 T_f}\right)} - e^{-\left(\frac{c}{\lambda_2 T_{b2}}\right)}}\right] \left[\frac{(1 - e^{-\alpha_1 l})}{(1 - e^{-\alpha_2 l})}\right] \tag{4.1}$$

The absorption coefficient α is different for the two transitions and is temperature dependent. If the (αl) product for the weaker line is maintained at a value on the order of 10 or greater, the final term of equation (4.1) reduces to one and a simpler expression for the peak height ratio can be written:

$$R = \left(\frac{\lambda_2}{\lambda_1}\right)^5 \frac{e^{-\left(\frac{c}{\lambda_1 T_f}\right)} - e^{-\left(\frac{c}{\lambda_1 T_{b1}}\right)}}{e^{-\left(\frac{c}{\lambda_2 T_f}\right)} - e^{-\left(\frac{c}{\lambda_2 T_{b2}}\right)}} \tag{4.2}$$

By monitoring two peaks simultaneously, the benefits of the two-temperature method are realized without sacrificing time resolution. The resulting method does not require adjustment of the background source. Temperatures above the maximum attainable source temperature can also be measured, and no operator interaction with the system is required.

4.3 Experimental Results and Discussion

The experimental setup has been described in Chapter 3. It is the same as that for traditional line reversal, except that a carefully selected color filter is placed between the background radiation source and the first lens. The lamp voltage is set to provide a background temperature consistent with the flame temperatures to be measured. For a known lamp voltage, lamp filament temperature can be determined from the calibration curve (Figure 3.10). Knowing this and the emissivity characteristics of tungsten, the filament brightness temperature at wavelength λ is:

$$T_b = \left\{ \frac{1}{T_{fil}} - \frac{\lambda}{C} \ln(\epsilon_{\lambda, T_{fil}}) \right\}^{-1} \tag{4.3}$$

When the lamp radiation is passed through the RG850 color filter, the apparent source temperatures at 852 and 894 nm will be lower than the temperature calculated in equation (4.3). The equation for T_{b1}, for example, is:

$$T_{b1} = \left\{ \frac{1}{T_{fil}} - \frac{\lambda_1}{C} \ln(t_{\lambda 1} \epsilon_{\lambda 1, T_{fil}}) \right\}^{-1} \tag{4.4}$$

When the lamp is operated at 100 V, for example, the resulting values are:

T_{fil} = 2492 K

T_{b1} = 2015 K

T_{b2} = 2115 K

Once T_{b1} and T_{b2} have been calculated from equation (4.4), a plot of R versus T_f is prepared based on equation (4.2). Three plots of

this type, corresponding to three different T_{b1} values, are shown in Figure 4.1. The curve representing a set of actual conditions is shown (lamp voltage of 100 V with an RG850 filter), along with two curves representing theoretical conditions for lower T_{b1} values (i.e. filters with lower transmissions at 852 nm).

Ideally, the method should be operated in the steepest region of the curve, where small temperature differences give rapidly changing peak height ratios. This means that the method is most accurate when T_f is in the region near T_{b1} and T_{b2}. At flame temperatures far below T_{b1} or far above T_{b2} the curve is too flat to use the method effectively. At higher lamp temperatures, and with the equipment used here, the useable range extends about 200 K above T_{b2}. The useable temperature range widens for larger differences between T_{b1} and T_{b2}, although spreads of more than about 600 K no longer change the curves appreciably. During actual temperature measurement, T_f is determined numerically rather than graphically.

Data were collected for two premixed flat flames. The premixed flat flame burner has been described in Chapter 3. Cool (<2200 K) flames were chosen so that verification using a Pt/Pt-Rh thermocouple would be possible. Both were rich CH_4/air flames, flame I at stoichiometric equivalence ratio ϕ of 1.7 and flame II at ϕ of 1.2.

At each flame position, 100 scans were made at a rate of one every 15 ms; the 100 scans were averaged to yield the reversal spectrum. A typical time-averaged scan is shown in Figure 4.2. This scan, taken with effective background temperatures of 1686 K and 1755 K, represents

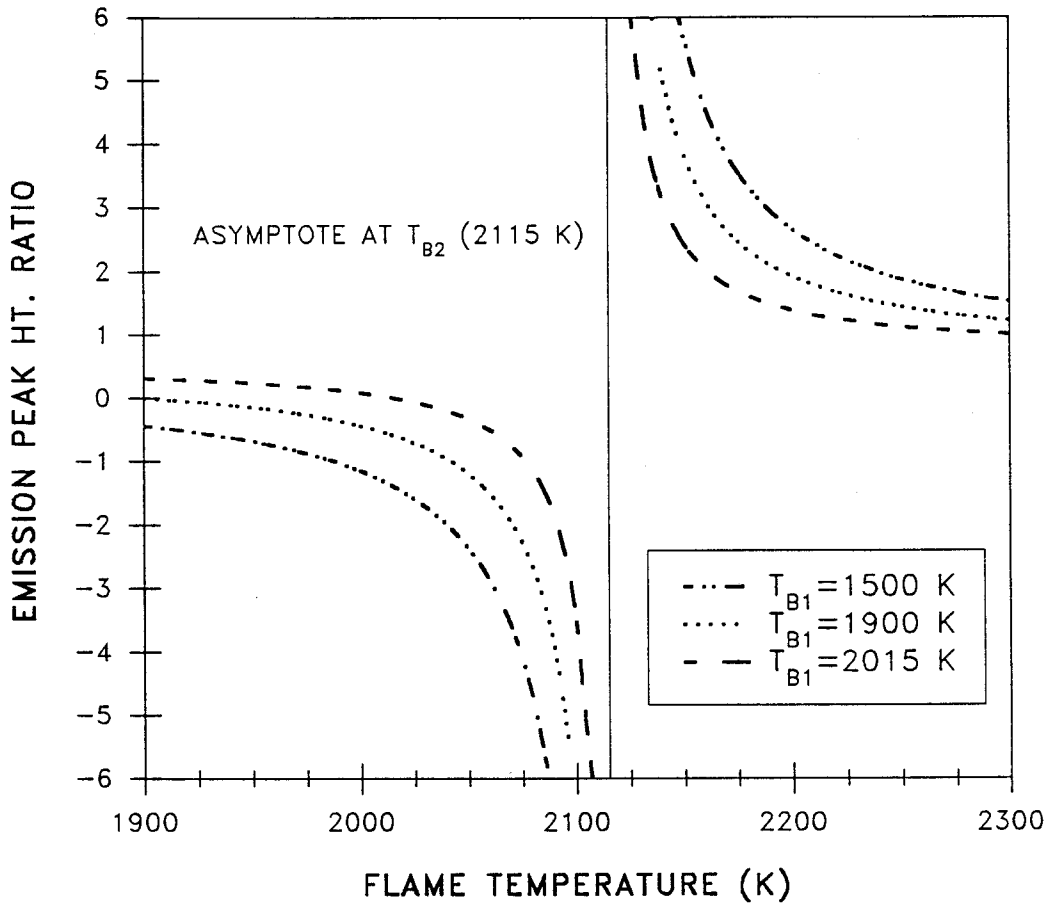

Figure 4.1 R vs. Flame Temperature for Various Values of T_{b1}

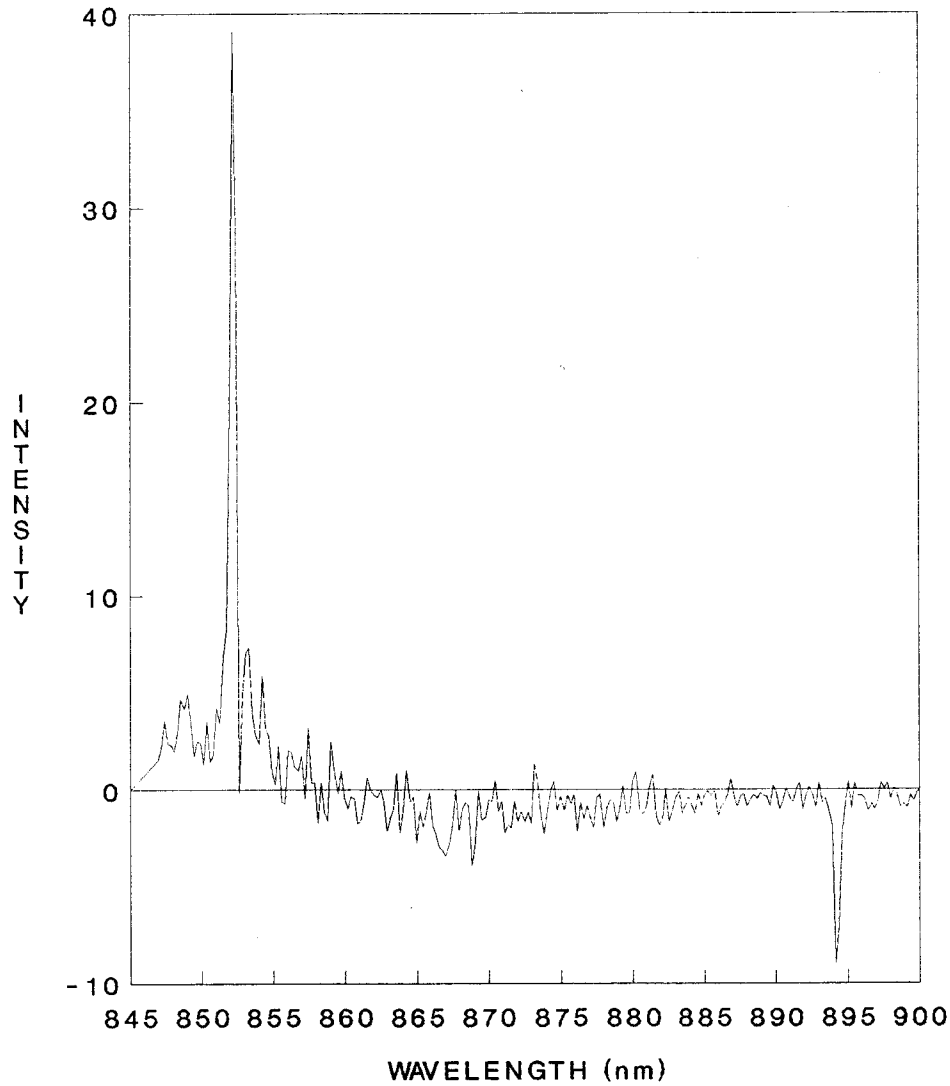

Figure 4.2 A Typical Time-averaged Spectrum

a flame temperature of 1707 K. Accordingly, the 852 nm peak is seen in emission ($T_f > T_{b1}$) while the 894 nm transition is in absorption relative to the background ($T_f < T_{b2}$).

Optically measured temperature profiles as a function of height above the burner surface are shown in Figure 4.3 for flames I and II. Corresponding thermocouple measurements for each flame, taken as described in Chapter 3, are included in the same figure. They have been corrected to account for radiation losses to the surroundings and losses due to conduction to the lead wires. Vertical error bars represent the uncertainty in the thermocouple data, most of which is due to the inability to precisely determine the emissivity of the thermocouple bead. The size of the symbols in Figure 4.3 has been chosen to correspond to the uncertainty in the optical measurements of $\pm$22 K. Calculation of the error associated with the optical measurements is discussed in Section 4.4.

Flame I represents temperatures near the lower limit of this method's useful range, for two reasons. First, below about 1700 K the number density of cesium atoms quickly falls to levels too low to provide an adequate signal. This is because most of the cesium is tied up in CsCl and CsOH at low temperatures. Second, lower temperature flames require using a lower source temperature for a given filter. At lower source temperatures the difference between T_{b1} and T_{b2} decreases, limiting the useful range of the method. This technique is therefore best suited to measuring temperatures between 2000 and 2800 K with a tungsten lamp as the background source.

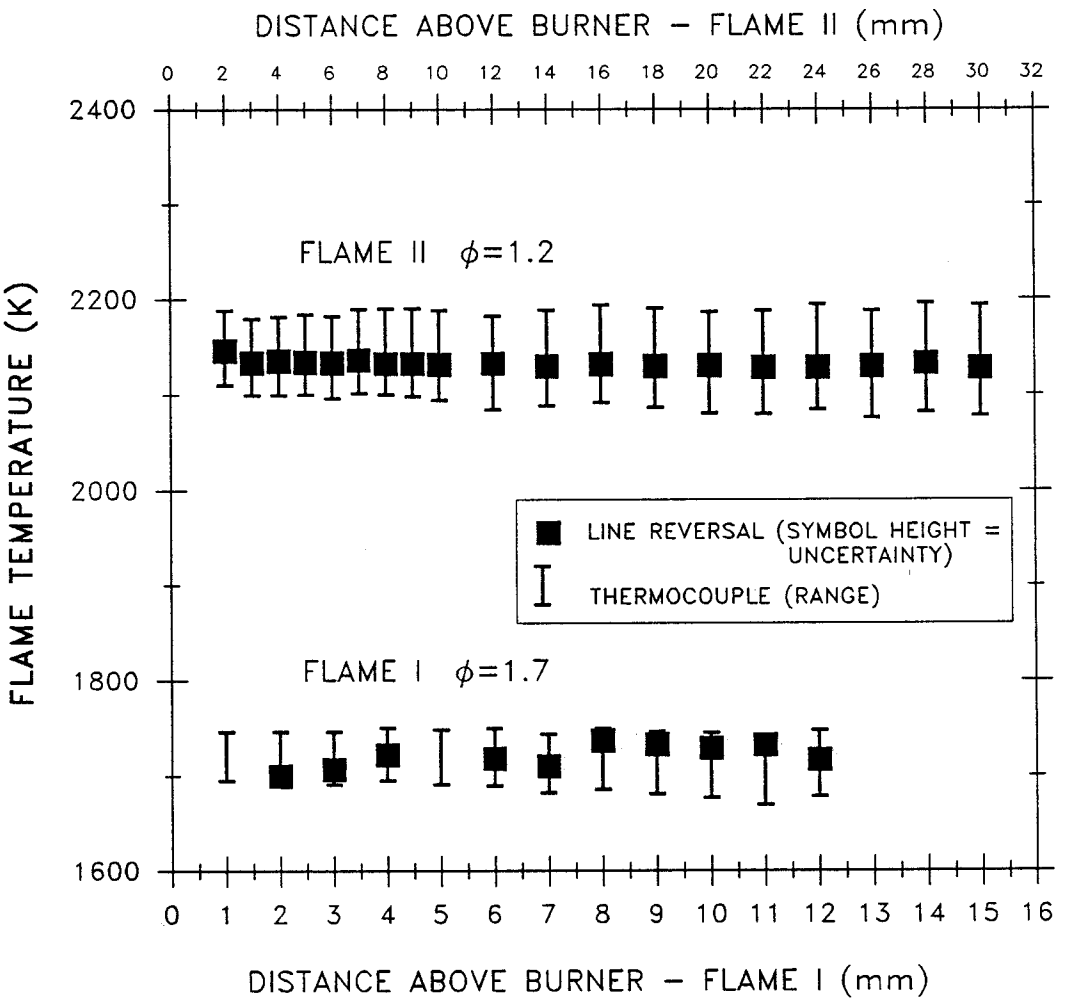

Figure 4.3 Experimentally Determined Temperature Profiles

One possible way to spread T_{b1} and T_{b2} and increase the working range would be to replace the color filter with an interference filter having about a 50 nm bandwidth. The interference filter could be tuned by rotation to give a variety of background temperature pairs.

4.4 Error Analysis

As previously stated, an assumed condition of applying equation (4.2) is that the (αl) product for the weaker transition must be maintained above about 10. For a flame diameter of 1 cm this corresponds to $\alpha \geq 10$ cm^{-1}. The absorption coefficient depends on oscillator strength and the number density of absorbing atoms, and for the limiting case it yields a required number density on the order of 3×10^{12} cm^{-3}. For cesium at 2500 K, approximately 1% of the cesium exists as free Cs atoms, the remainder being tied up primarily in CsCl and CsOH. The total cesium concentration for the limiting case is therefore approximately 3×10^{14} cm^{-3}, which corresponds to a minimum mole fraction of about 10^{-5} in the inlet gas stream. This is about two orders of magnitude below the number density obtained when a cesium solution is atomized into the inlet gas. As such, minimum seed density is not likely to be an issue in application of this method, except in the case of very thin flames. The sufficiently large (αl) product also eliminates any effect of temperature on excited state populations. Although temperature dependent population differences would affect the relative absorption coefficients at the two transition wavelengths, both values are always large enough that their effect on the ratio calculation in equation (4.2) is negligible.

In the experiments reported here, the filament temperature calibration represents the greatest uncertainty. The calibration is sensitive to accurate knowledge of tungsten emissivity for the actual filament, correct filter transmittance values over all wavelengths, and the transmission characteristics of the quartz envelope. There is also uncertainty in the peak heights which affects the ratio used to calculate flame temperature. Using the method of Kline and McClintock (1953), these errors can be traced to determine their effect on the final temperature calculation. In the worst case, lamp voltages between 60 and 90 V have errors in the filament temperature of ±30 K. This affects the two background brightness temperatures T_{b1} and T_{b2} through equation (4.4). The uncertainty in the brightness temperature can be found from

$$\frac{w_{Tb}}{T_b} = \left\{ 1 - \frac{\lambda T_{fil}}{C} \ln(t_\lambda \epsilon_{\lambda, T_{fil}}) \right\}^{-1} \left(\frac{w_{Tfil}}{T_{fil}} \right) \tag{4.5}$$

In the range of values being used here, the resulting uncertainty in the two brightness temperatures is ±24 K. Both temperatures will be in error in the same direction, however, and this lessens the ultimate effect on the final flame temperature. The result will also depend to a great extent on the region of operation on the R vs. T curve. Because equation (4.2) cannot be solved analytically for T_f as a function of R, conventional methods cannot be used to estimate the uncertainty in T_f due to that in the two brightness temperatures. For the values reported here, the numerical solution of R was repeated for several measurements with T_{b1} and T_{b2} varying over the range of their uncertainty. The resultant uncertainty in the final flame temperature is estimated at ±15 K when the lamp is operated in the region corresponding to the flame I and II measurements.

The error in R caused by the uncertainty in measurement of the peak heights will also vary depending on the region of operation on the curve. The peak at 894 nm has the greater uncertainty due to decreased detector sensitivity, as described in Section 3.5. For the measurements reported here the 894 nm peak height uncertainty is estimated at ±10%. The resulting effect on reported flame temperature is approximately ±7 K.

The accuracy of the final results depends on the steepness of the R versus T_f curve in the area of operation. If the flame temperature is far below T_{b1} or far above T_{b2}, accuracy is sacrificed. Ways to improve the operating range by increasing the spread between T_{b1} and T_{b2} were discussed in Section 4.3. As long as care is taken to operate within the prescribed region, the relative change in R for a given temperature change will be large enough to make this a negligible source of error.

Thomas (1968a) and others (Daily and Kruger, 1976) have discussed the effects of a cool boundary layer on the final results of line reversal temperature measurements. Where thick boundary layers exist, corrections are possible to account for the increased absorption (Strong and Bundy, 1954b). The effect of a cool boundary layer is to reabsorb the radiation emitted at the center of the line. However, cooler gases have a much lower cesium atom concentration and this weakens the effect. Because both peaks are affected to the same extent, the peak ratio is not substantially changed. This is an advantage over traditional line reversal, where self absorption caused by a boundary layer affects the source balance point. For the experimental data reported here, flat

flames were used with temperatures that vary little in the transverse direction. The contribution of boundary layer effects was negligible compared to the overall error.

4.5 Conclusions

Using a filtered reference source and monitoring two closely spaced transition lines, flame temperatures can be determined by line reversal without balancing the source. Flame temperatures as much as 200 K higher than the source brightness temperature can be measured, and the system can be fully automated without sacrificing temporal resolution. Errors can be minimized by using an accurately calibrated reference source and selecting filters carefully. The method is well suited for measuring cesium-seeded flames. Other Group IA elements can also be used with appropriate choice of filter, spectrograph grating density, and detector sensitivity.

5. CHARACTERIZATION OF ELECTRICAL DISCHARGES THROUGH SEEDED DIFFUSION FLAMES

5.1 Introduction

In Chapter 6, a study of Lorentz-induced mixing of planar diffusion flames will be described in detail. However, this study first requires an understanding of how flames behave when subjected to strong electric fields. Extensive work with electric currents in premixed flames has been reported in the literature, but the current-carrying properties of planar diffusion flames have not previously been characterized. In this chapter the results of an investigation of the electrical characteristics of a cesium-seeded methane/oxygen diffusion flame are reported. The effects of electrode gap and location downstream of the burner exit plane are examined. Predictions of the expected temperature rise during each arc mode are made based on theoretical considerations; optically measured temperatures in the discharge region are reported and compared with predicted values.

5.2 Experimental Results and Discussion

The burner used in this study is the planar diffusion burner which was described in Chapter 3. Parallel streams of methane and oxygen issue from long, narrow slots with equal velocity. A shroud of inert gas surrounds the reactants to stabilize the flame and prevent interaction with room air. An electric potential is applied across graphite electrodes located downstream of the burner exit plane.

During early experiments, it quickly became apparent that there were two distinct modes of operation of the electrical discharge. This is similar to the observations in premixed flames that were reported by

Ulherr and Walsh (1971), who dubbed the lower current discharge "mode A" and the higher current discharge "mode B." Although there are some differences between these mode descriptions and those observed in the diffusion flames, enough similarities exist to warrant adoption of the same nomenclature to differentiate the two types of discharges observed in this study. The electrical characteristics of the two discharge modes are quite different. Although both modes will be discussed here, the higher current B mode is of primary interest and its properties will be emphasized.

As the electric field across the flame is gradually increased from 0, there is no observed change or significant current flow until an applied voltage between 230 and 320 V is reached (depending on the electrode position). At this point the A mode discharge begins at currents of 30 to 80 mA. The same behavior that Ulherr and Walsh reported is seen, with a small bright spot which appears to flicker around on the anode surface. As the voltage is increased the current increases linearly until a sudden transition to the B mode discharge occurs. A five- to ten-fold current increase is seen and the appearance of the discharge changes considerably. Whereas the visible portion of the B mode discharge in premixed flames extends completely between the electrodes, in the diffusion flame it does not. An extremely bright region surrounds the cathode and extends approximately 1/3 of the way across the electrode gap. A less intense bright spot is seen at the anode. As the applied voltage is increased, the bright region extends farther across the gap, but it never bridges the gap entirely. In a few configurations with a very small electrode gap, a third mode corresponding essentially to a short circuit was occasionally established. Here the conductivity

of the gases rose sharply with increased temperature, yielding an extremely high current arc between the electrodes with almost no voltage drop. This type of high temperature contracted arc is described by Karlovitz (1962). This behavior is quite undesirable due to its limited practical use, and it was avoided during these experiments.

In premixed flame studies, the most important electrode parameter is the gap between the anode and cathode. The geometry of these systems is usually such that the electric field is oriented parallel to the flow direction, so increased gap corresponds to the anode being positioned farther downstream. In the present configuration, however, the field is aligned perpendicular to the flow direction. Thus, in addition to gap length, another important parameter is the location of the electrodes downstream of the burner exit. This distance relates to a characteristic time in the development of the flame region.

In any discharge system, a voltage drop occurs at either or both electrodes. Because the total applied voltage across the electrodes is measured, it is necessary to estimate the fraction of this total which takes place across the flame itself. The method used in this estimation is that described by Fells et al. (1967) in their premixed flame study. For a fixed value of flame current, the total applied voltage is plotted versus electrode gap. This is a relatively flat linear relationship which, when extrapolated to zero gap, yields the voltage drop associated with the electrodes alone. Figures 5.1 and 5.2, for modes A and B respectively, show the extrapolations used to determine electrode drop. Despite the much larger currents measured in the B mode, the electrode drops are in the same range as for the A mode. The drop voltage increases linearly with current for both modes in the range of interest,

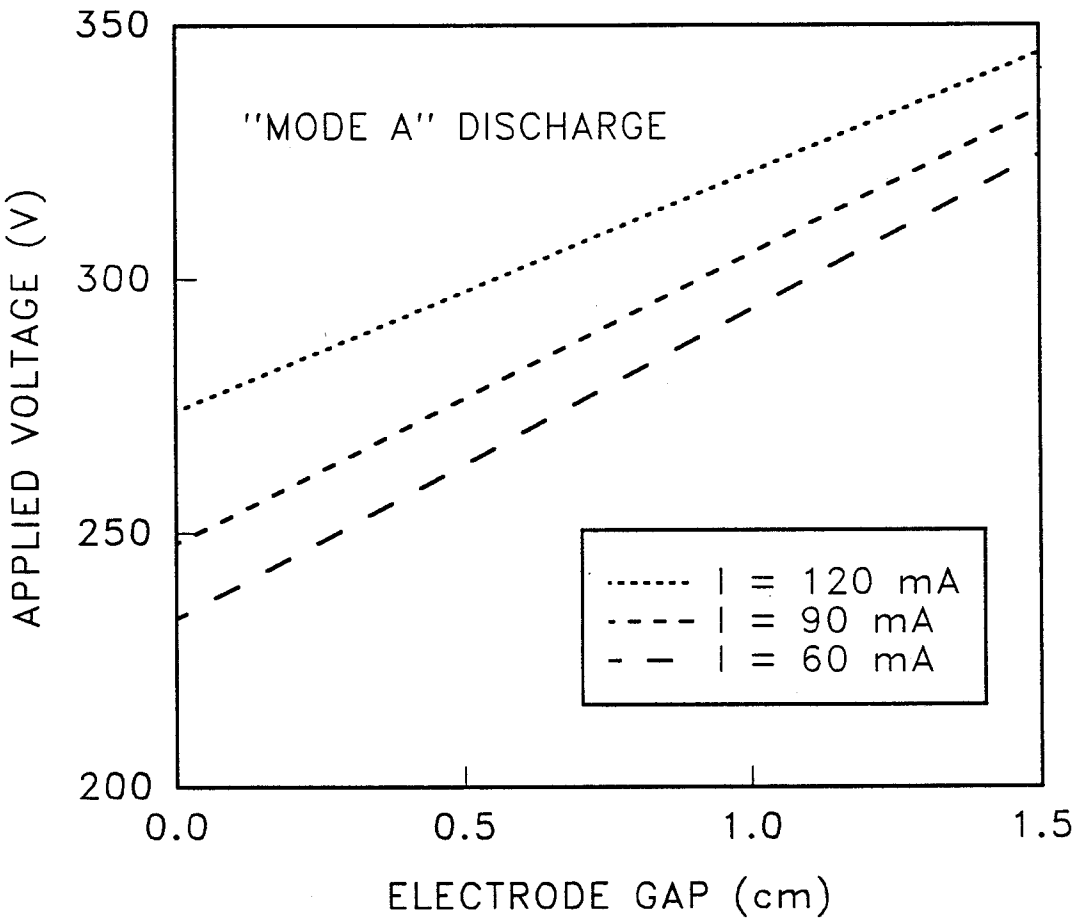

Figure 5.1 Calculation of Electrode Fall Voltage for Mode A

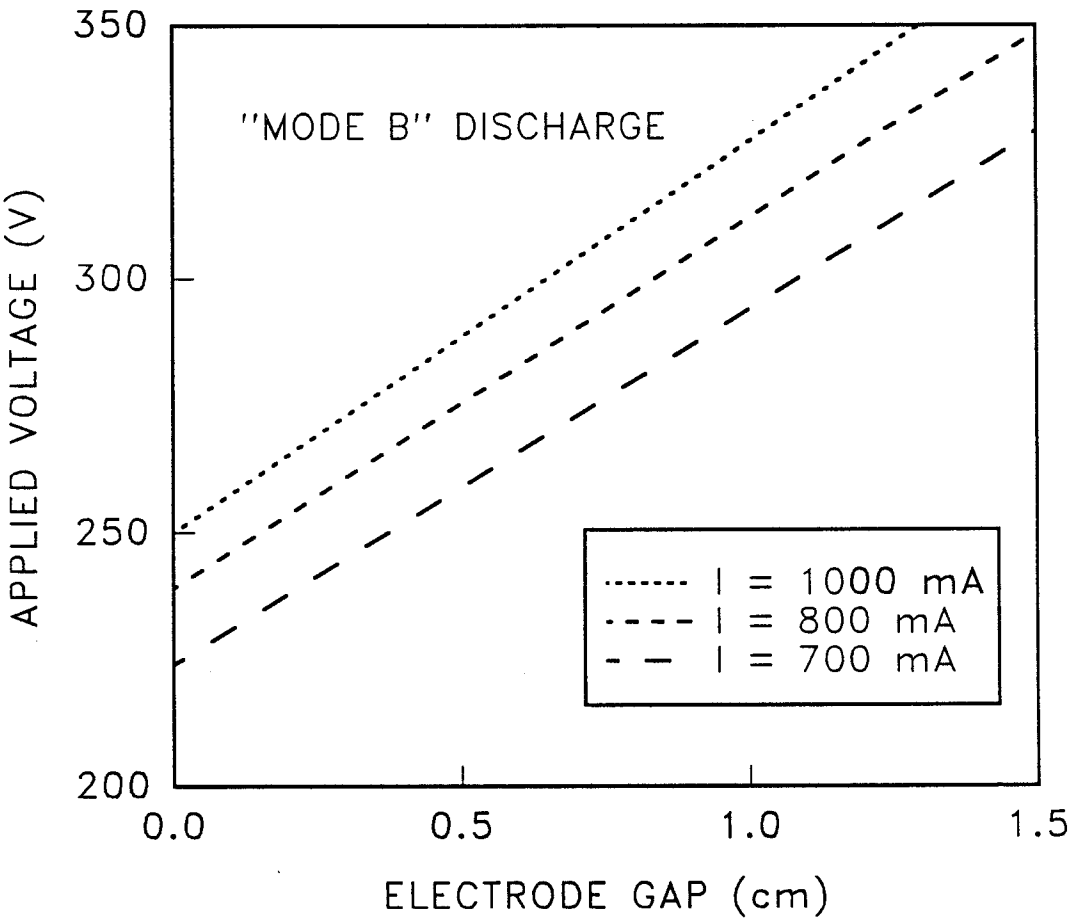

Figure 5.2 Calculation of Electrode Fall Voltage for Mode B

as shown in Figure 5.3. This differs from observations reported in premixed flames (Fells et al., 1967; Ulherr and Walsh, 1971) where anode fall voltage was seen to decrease slightly with increased current. In both cases, however, the effect is small relative to the overall electrode drop.

The voltage-current characteristic curves reported in the literature for premixed flames vary widely. In some cases the slope is positive (Lapp and Rich, 1963) while in others it is negative (Ulherr and Walsh, 1971). The variation in reported behavior can be explained on the following basis. Initially current increases from zero approximately according to Ohm's law, giving a positive slope. At higher currents, Joule heating of the gas column raises its conductivity to the point where an increase in current is obtained at nearly constant voltage, and the characteristic flattens. At larger currents, the conductivity increases at a higher rate and a negative slope is observed.

In the diffusion flame experiments described here, the characteristic is positive and quite linear in the region studied, as shown in Figure 5.4. This is again attributable to the orientation of the electric field transverse to the gas flow direction. The region through which the discharge passes is continually being filled with fresh gases while Joule heated gases are swept downstream. This configuration precludes the buildup of energy in the arc region which is necessary for development of temperatures (and thus conductivities) high enough to give a negative voltage-current characteristic.

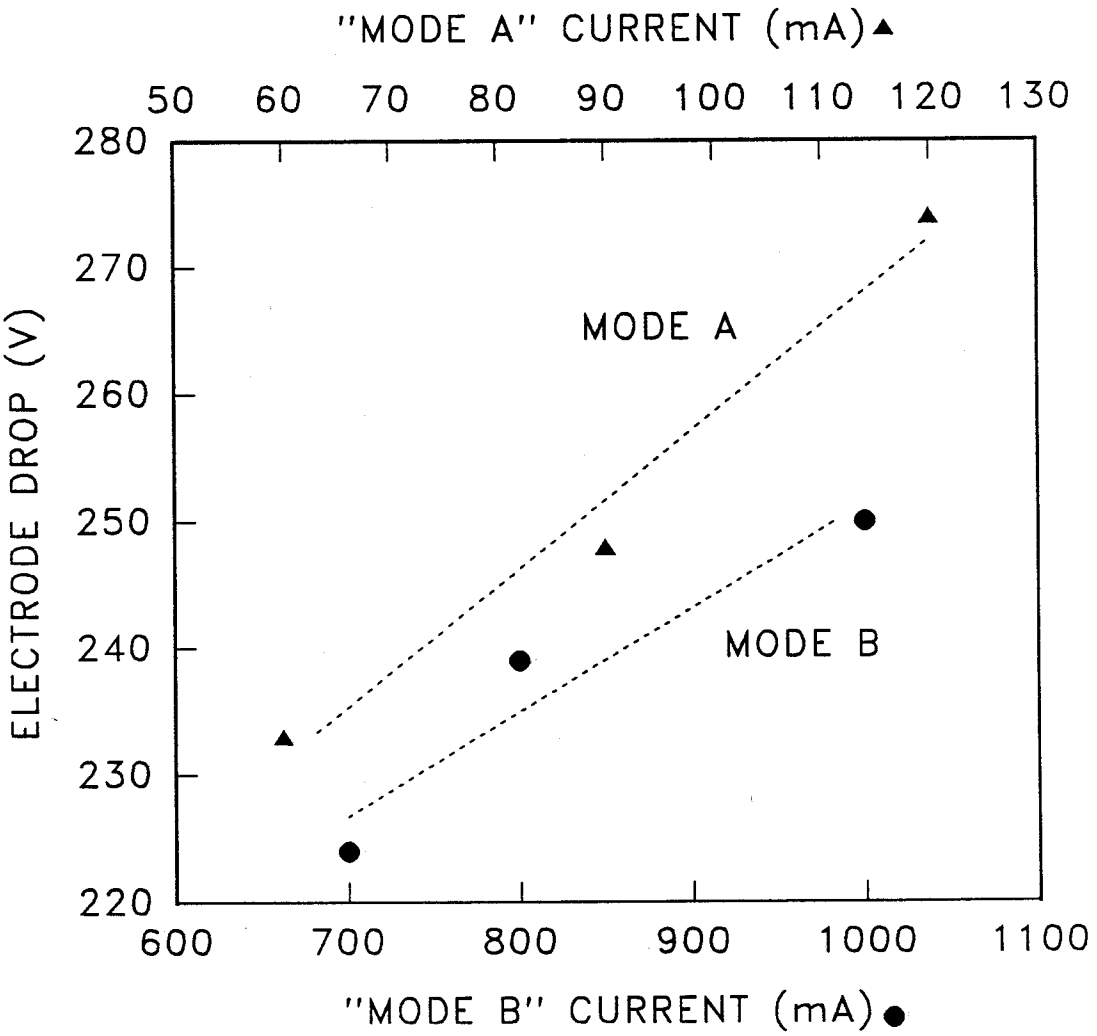

Figure 5.3 Electrode Fall Voltage versus Current, Modes A and B

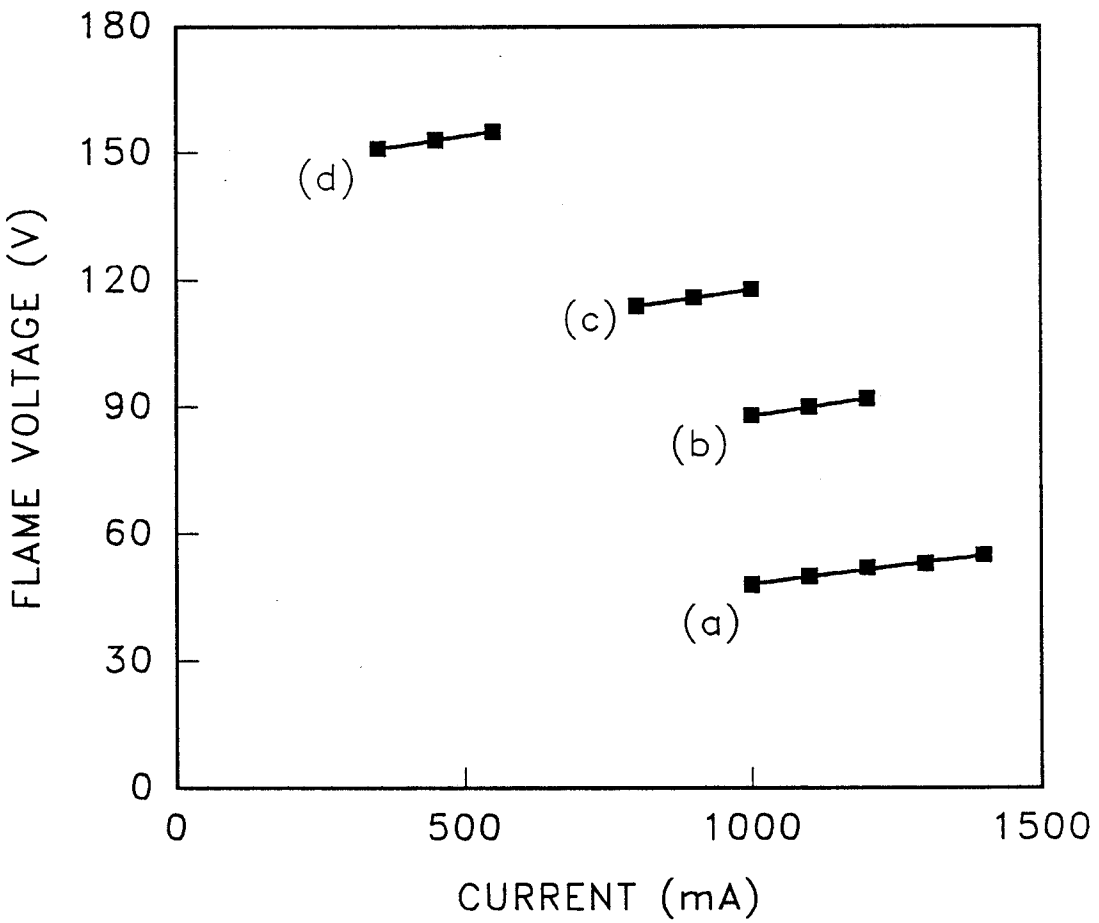

Figure 5.4 Voltage-current Characteristics for Mode B (a) gap=1 cm, x=1 cm; (b) gap=1 cm, x=0.7 cm; (c) gap=1 cm, x=0.4 cm; (d) gap=1.5 cm, x=0.4 cm

It is interesting to note that the continual sweeping of conductive gases downstream causes the hottest flame region to occur not directly between the electrodes, but several mm downstream. This hotter region is more conductive, and the path taken by the discharge is determined by a balance between higher conductivity and greater path length. This behavior is confirmed with temperature measurements and is discussed in more detail later in this section.

In Figure 5.4 the experimentally obtained voltage-current characteristics of the B mode are plotted for several electrode configurations. Because of uncertainty about the cross-sectional dimensions of the discharge region, flame current is plotted on the abscissa instead of current density. Voltages are those across the flame only. The three lower curves represent a constant gap of 1 cm, with the location downstream of the burner exit plane varied from 0.4 to 1 cm. The conductivity of the gas increases farther from the exit as the flame develops, its temperature increases, and the zone of hot reactants and products grows in size. Plotted in the top curve of Figure 5.4 for comparison is the curve obtained when the electrode gap was increased to 1.5 cm. These data were taken at the position closest to the burner exit (x=0.4 cm). As expected, this increases the voltage required to sustain a given current because the path length (and thus total resistance of the flame) increases. Characteristic curves for the A mode exhibited similar behavior as a function of electrode location, although the slopes of the lines were less consistent than those seen in the B mode.

Because they carry substantially different currents at similar voltage drops, one of the major differences between the two discharge modes is the power input to the flame. This results in type B flames having temperatures much higher than type A flames do in the region near and downstream of the electrodes. Theoretical prediction of flame temperatures is rendered difficult by the complexity of the flame geometry, interaction with the electrodes (which themselves lose heat by conduction), and uncertainty about the cross-sectional dimensions of the current path. It is useful, however, to make simplifying assumptions and estimate the expected flame temperature in the discharge region for both modes.

The total power input to the flame is easily calculated from the voltage/current measurements. The crucial question is whether the voltage drop considered should be that through the flame alone, or the total voltage including the electrode drop. Lapp and Rich (1963) estimated temperatures in premixed flames by considering the two voltages as bounding values. They found that at lower power inputs it was more appropriate to disregard the electrode drop, while the contribution of the electrode drop was sizeable at higher power inputs. In the diffusion flame, the electrodes sit near the flame edge and extend beyond the flame into the surrounding inert shroud, so there is considerable heat loss via conduction. The electrode drop voltage probably results mainly in energy input to the electrode surface, which increases the conductive loss and results in little net enthalpy increase in the flame. The lower voltage (corresponding to the drop through the flame alone) is therefore used to estimate flame temperatures. Two different approaches

are taken in making these estimates, but each gives a reasonable prediction of the experimentally measured temperatures. Calculations are made for typical discharges of 100 mA/50 V for mode A and 1000 mA/50 V for mode B.

From the total power input, the average temperature rise of a volume of gas can be calculated knowing its heat capacity:

$$\int \dot{m} C_P dT = iV \tag{5.1}$$

The problem is determining what mass flowrate should be considered. The gases flowing through the relatively thin discharge region are not the only ones being heated, since there is considerable heat transfer to the neighboring methane and air streams. Considering the total mass flowrate for the CH_4, O_2, and N_2 would give an unreasonably low estimate of the temperature increase in the discharge region, since the input energy is not uniformly distributed across the entire flow region. The mass flowrate is therefore taken as that of the reactants (neglecting the inert gas) and is 0.04 g/s, which is expected to yield an average temperature increase for the reactants. Although the heat capacity is a function of temperature, it varies less than 4% from the mean value (2.1 J/g-K) in the region of interest, so temperature dependence is neglected. This results in a ΔT of 60 K for the type A discharge and 595 K for the type B discharge. Increases larger than the calculated values would be expected near the discharge. In the unburned reactant flowstreams farther from the flame, the temperature increase should be lower than the calculated value.

As an alternate approach, the power input can be compared to the enthalpy of combustion of the original reaction. The enthalpy increase results in a higher theoretical temperature, which can be calculated. Corrections can then be made to take into account the fact that the actual flame is below this theoretical temperature, owing to its small size and substantial end losses.

It is first necessary to estimate the fraction of the total CH_4 inlet mass flowrate that is consumed in the region of the flame sheet influenced by the discharge. Referring to the geometry in Figure 5.5, the mass diffusion rate of methane into the flame sheet is:

$$\frac{d\dot{m}_{diff}}{dA} = D_{CH4}\frac{\rho^*_{CH4}}{(s/2)} \tag{5.2}$$

For unit depth into the page, a differential amount of mass $d\dot{m}$ flows through a differential area $dA=(1)(dx)$. Equation (5.2) is integrated to yield:

$$\dot{m}_{diff} = \frac{2D_{CH4}\rho^*_{CH4}}{s}(x_2-x_1) \tag{5.3}$$

The fraction of the total methane mass flowrate consumed between positions x_1 and x_2 downstream of the exit plane is:

$$\frac{\dot{m}_{diff}}{\dot{m}_{CH4}} = \frac{2D_{CH4}\rho^*_{CH4}(x_2-x_1)}{\rho^\circ_{CH4}u^\circ_{CH4}A_{slot}s} \tag{5.4}$$

Using the method of collision integrals and Lennard-Jones potentials (Cussler, 1984) the diffusion coefficient of methane into the flame zone (D_{CH4}) is calculated as 8 cm^2/s. The flame zone thickness s is approximately 0.5 cm, and the volumetric flowrate $u^\circ_{CH4}A_{slot}$ is 20 cm^3/s. The discharge height (x_2-x_1) is estimated at 0.7 cm and ρ^*_{CH4} is measured

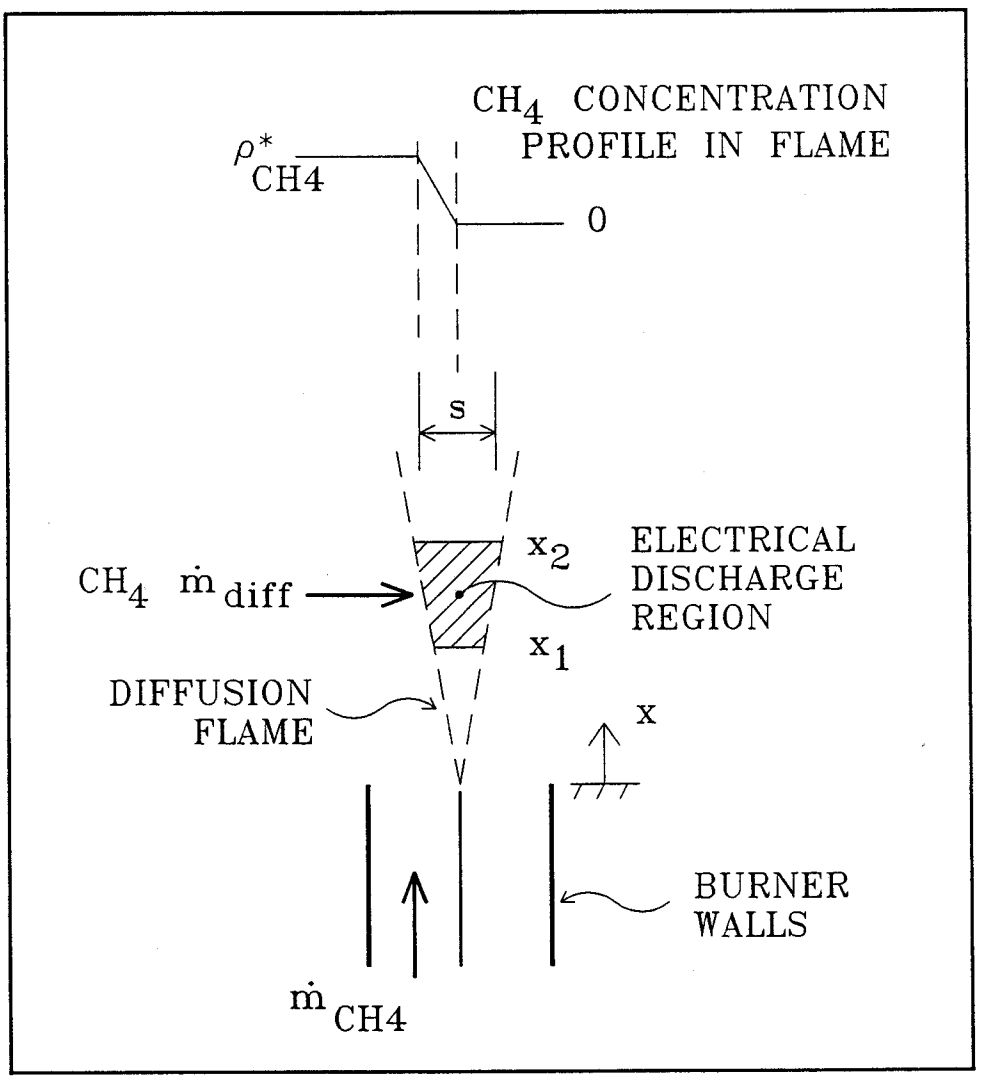

Figure 5.5 Diffusion of Methane into the Flame Zone

at 2100 K. From equation (5.4), approximately 16% of the methane is consumed in the region of the discharge. The power input from the discharge is converted to a rate per unit mass which is added to the enthalpy per unit mass of products in the flame reaction. A correction is made for losses which lower the flame temperature below its theoretical maximum and a new temperature is calculated from equilibrium considerations. The resulting ΔT is 100 K for the mode A case and 635 K for the mode B case. These estimates are of the same order as those calculated above by considering an increase in bulk enthalpy.

Actual temperature measurements compare well with the predictions. The flame temperature just above the electrodes was measured with no discharge and under conditions of each discharge mode. Under conditions of no discharge, the method described in Chapter 4 was employed. Using simultaneous monitoring of the cesium doublet at 852 and 894 nm, the flame temperature was measured at 2340 K. For temperature measurements during the discharges, a different approach was used. First, the intensity of the 852 nm emission peak was recorded at the known flame temperature of 2340 K. With the discharge established, the intensity of the same peak was again determined. If sufficient optical depth is insured (e.g. by viewing the flame from its end) an estimate of the discharge temperature can be obtained from the ratio of the two intensities:

$$T_d = \left[\frac{1}{T_f} - \frac{\lambda}{C} \ln\left(\frac{I_d}{I_f} \right) \right]^{-1} \tag{5.5}$$

Figure 5.6 shows superimposed emission versus wavelength curves for the three cases (no discharge, and A and B mode discharges). From the intensity ratios and equation (5.5), mode A and B temperatures are 2465 K and 3020 K, respectively. The measured mode A ΔT is thus 125 K,

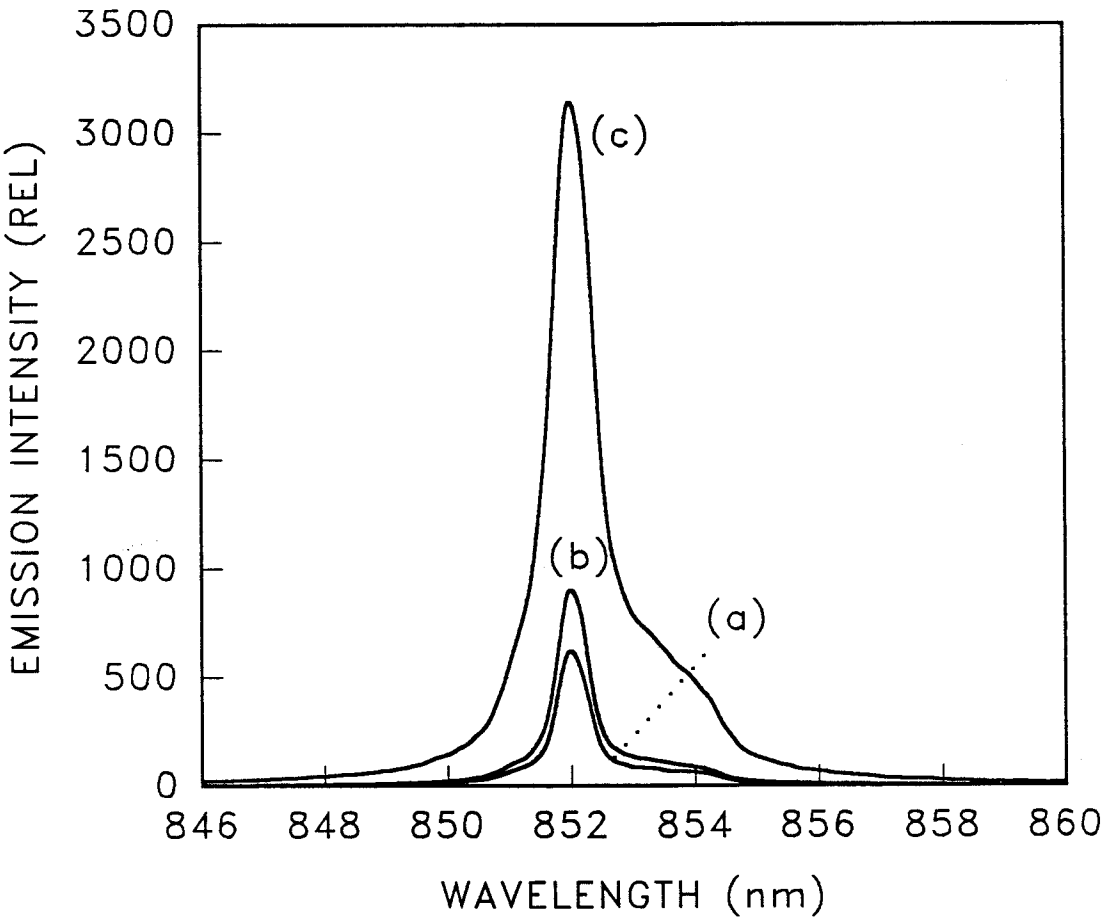

Figure 5.6 Emission Spectra of Flame With (a) No Discharge; (b) Mode A Discharge; (c) Mode B Discharge

compared with estimated values of 60 K and 100 K by the two methods. For the mode B discharge ΔT is measured at 680 K, versus estimates of 595 K and 635 K.

It was previously mentioned that the hottest region of the flame is not located directly between the electrodes, but downstream slightly. This is due to the Joule heated gases constantly being swept downstream of the discharge volume. The burner configuration precludes optical temperature measurement parallel to the flame sheet in the zone directly between the electrodes. The flame temperature about 1 mm above the top of the electrodes is the closest measurement possible. Optical temperature measurements perpendicular to the flame sheet were attempted, but the optical depth was not sufficient to provide meaningful quantitative results. Qualitatively, however, it could be seen that the cesium emission intensity was a maximum approximately 5 to 6 mm downstream of the electrode centerline.

5.3 Conclusions

When an electric field is imposed across a planar diffusion flame, the resulting current discharge can take on two different forms. Both the low and high current modes exhibit similar electrical characteristics, with the latter sustaining current about an order of magnitude larger than the former. The most important electrode parameter is position downstream of the burner exit plane. At locations very near the exit, the flame has not developed sufficient temperature to conduct effectively. The effect of increasing electrode gap is quite predictable because the planar flame is essentially uniform in the field direction.

Estimates of the temperature increase during discharge, made with two different approaches, give a reasonable prediction of the measured values. The high current B mode discharge results in a much greater power input to the flame and thus substantially higher flame temperatures than the low current A mode.

6. LORENTZ-ENHANCED MIXING OF SEEDED DIFFUSION FLAMES

6.1 Introduction

Diffusion controlled burning is one way of releasing the heat necessary for energy generation, propulsion, and space heating. The rate of combustion at the interface between co-flowing, laminar streams is controlled by molecular diffusion into the flame zone. To improve the combustion rate, "bulk" mixing of the reactants must be introduced. Typically this has been accomplished by inducing turbulence through some physical method (e.g. placing a rod in the reactant stream), thus enhancing the transport of the reactants to the interface. However, it may be preferable at times to promote this bulk movement of reactants without physically invading the flow stream. One means of accomplishing this is with externally applied electric and magnetic fields.

The bulk mixing referred to in this chapter is the movement of one reactant into the region occupied by the other. Molecular mixing still takes place at the interface. However, to enhance the overall combustion rate there must be macroscopic movement of one of the reactants into the other. At the flame sheet interface between two co-flowing reactants, this bulk mixing may be induced by "wiggling" the interface. This would lead to small, alternate displacements of the fuel and oxidizer and result in an inter-penetration of these reactants. Alternately, if large displacements of the flame sheet can be achieved the inter-penetration will result in bulk transport of one of the reactants into the other, providing mixing on the macroscopic scale.

To accomplish this type of mixing, a body force must be generated on the gases within the flame sheet. If the electrical conductivity of the gas is sufficiently high it can act as a conductor and carry current. The flame can therefore be subjected to induced body forces in the same manner as a copper wire when an appropriately oriented magnetic field is present. A technique has been investigated which exploits this effect to oscillate a planar diffusion flame. The result is an enhanced mixing effect using only non-invasive, externally applied fields.

6.2 Theoretical Development

Figure 6.1 depicts a volume of gas (or section of a flame sheet) under the influence of a transverse Lorentz force. It will be accelerated until some terminal lateral velocity is reached, representing a balance between the induced body force and an opposing drag force.

The magnitude and direction of the Lorentz body force are given by the vector cross product of the current density (**j**) and the magnetic flux density (**B**):

$$\mathbf{f}_{Lorentz} = \mathbf{j} \times \mathbf{B} \tag{6.1}$$

In the present case, calculation of the **j x B** force is straightforward because the current direction and magnetic field lines are at right angles to one another. The magnitude of the force experienced by the volume of ionized gas is

$$F_{Lorentz} = jBV = \left(\frac{i}{bs}\right)B(slb) \tag{6.2}$$

The physical dimensions of the gas volume undergoing the acceleration are shown in Figure 6.1.

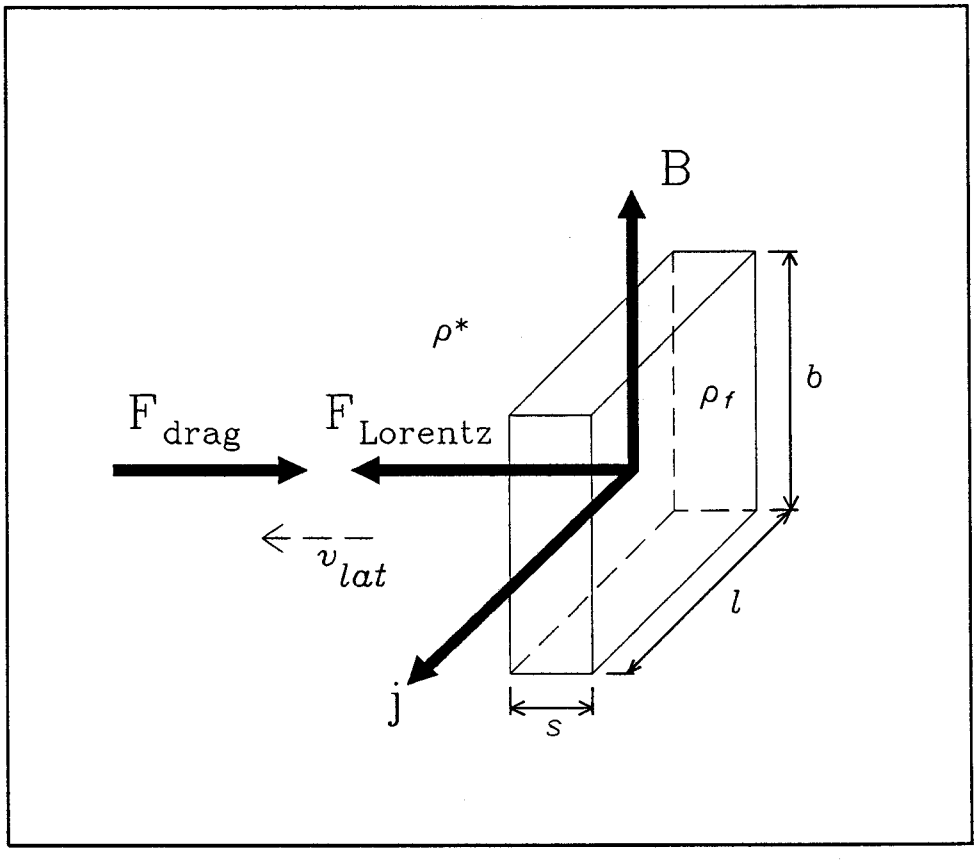

Figure 6.1 Flame Sheet Under the Influence of a Transverse Lorentz Force

The force opposing this **j x B** effect comes from drag on the moving flame sheet. Assuming the sheet to be impermeable, the drag force is given by

$$F_{drag} = A_p C_D \frac{\rho^* v_{lat}^2}{2} = (lb) C_D \frac{\rho^* v_{lat}^2}{2} \tag{6.3}$$

where ρ^* is the density of the gas through which the flame is moving and v_{lat} is the lateral velocity with which the flame moves. The lateral acceleration can then be found by dividing the difference between the above two forces by the mass of the volume element:

$$a_{lat} = \frac{iB}{\rho_f sb} - \frac{\rho^* C_D v_{lat}^2}{2\rho_f s} \tag{6.4}$$

This acceleration is simply the time derivative of v_{lat}. If a period of time which is short relative to the oscillation period of the current is analyzed, the time dependence of the current can be neglected. A small time interval when the current is near its maximum value (i_{peak}) will be considered. The validity of this assumption will be verified after the final relation has been derived. Equation (6.4) is separated and integrated to yield

$$\int_0^{v_{lat}} \left(\frac{i_{peak} B}{\rho_f sb} - \frac{\rho^* C_D v_{lat}^2}{2\rho_f s} \right)^{-1} dv_{lat} = \int_0^t dt \tag{6.5}$$

Note that the drag coefficient is treated as a constant in this development. In order for this to be valid, an appropriately averaged value for C_D must be used. Equation (6.5) is integrated to yield an expression for the final lateral velocity of the gas after it passes through the current-carrying region, assuming it starts from rest:

$$v_{lat} = \left(\frac{2 i_{peak} B}{b \rho^* C_D}\right)^{\frac{1}{2}} \tanh\left(\frac{\rho^* C_D i_{peak} B l^2}{2 \rho_f^2 s^2 b}\right)^{\frac{1}{2}} \tag{6.6}$$

The first term on the right represents the terminal velocity of the flame sheet given a sufficiently large accelerating distance. The second term takes into account the finite time required for this acceleration. For values of the tanh argument greater than four, the resulting expression simply reduces to the terminal velocity of the flame sheet. For the experiments described here, the time required to reach terminal velocity from rest is on the order of 0.002 s. The total time that a volume of gas is exposed to the driving force depends on the exit velocity of the reactant gases from the burner, and is on the order of 0.020 s in these experiments. It is therefore quite reasonable to assume that terminal velocity is reached.

The expression in equation (6.6) can now be used to verify the assumptions made when equation (6.5) was integrated. If the terminal value is quickly achieved, the lateral gas velocity will track the current with little lag. This is the case in the present analysis. An appropriately averaged current during the time the conductive gas volume is under acceleration can therefore be used in the derived relationship. During the integration the maximum value (i_{peak}) was used, which will be shown to be a reasonable assumption. The period of time that will be used in the flame analysis is the shortest allowed by the video recording method. For this study, time periods as short as 0.002 s could be analyzed (this is discussed in more detail in the next section). The period of the alternating current is 0.0167 s, so during a 0.002 s span centered about the maximum its value will be nearly constant and close

to its peak value. The small error which is introduced by making the simplification that current is constant at its peak value is quantified in Section 6.4.

To examine the variation of v_{lat} with magnetic flux density, a new variable is defined:

$$\eta = \left(\frac{2 i_{peak}}{b \rho^{*} C_D} \right)^{\frac{1}{2}}$$

Rewriting equation (6.6) in terms of η :

$$v_{lat} = \eta B^{\frac{1}{2}} \tanh \left\{ \left(\frac{i_{peak} t}{\eta \rho_f s b} \right) B^{\frac{1}{2}} \right\} \tag{6.7}$$

From this expression, the maximum lateral velocity varies with the square root of B, with all other parameters held constant:

$$v_{lat} = \eta B^{\frac{1}{2}} \tag{6.8}$$

6.3 Experimental Results and Discussion

To produce the forces necessary for enhanced mixing the magnetic and electric fields must be properly oriented relative to the gas flow. A magnetic flux density of up to 0.035 T (350 gauss) is generated by the external coil (described in Chapter 3) such that the **B** lines run parallel to the gas flow. An electric field is applied across graphite electrodes positioned near the burner exit. The electrodes extend into the flame sheet, where the gas conductivity is high enough for about 1 A of current to flow at a total applied voltage of 220 V. With this configuration the Lorentz force generated on the flame sheet is normal to the flow, and is consequently directed so as to promote bulk movement of the

reactant streams into one another. Application of an a.c. voltage across the electrodes results in a time-varying Lorentz force which acts to move the flame sheet alternately toward the fuel and the oxidizer streams. For these experiments the field was generated with a 280 V Variac with an oscillation frequency of 60 Hz.

Once a seeded diffusion flame was initiated at the burner exit, the a.c. voltage across the electrodes was gradually increased until a current path was established through the flame, usually at about 280 V. Once the conduction path was initiated and the graphite electrodes heated up the voltage could be decreased, with the total applied potential across the electrodes being about 220 V rms. The current through the electromagnet was then gradually increased from 0 to 0.032 T (0 to 320 gauss) during an experiment, which lasted about 30 seconds.

During the experiments the flame sheet was oscillated at 60 Hz, so its shape could not be discerned visually. To record the effects of the Lorentz force a high-speed video camera was used to capture images of the flame while the magnetic field was increased to its maximum value. The video system has been described in Chapter 3. The recordings were then replayed at a slower rate for analysis of the events of interest and to confirm the existence of the predicted behavior. Additionally, the video footage was analyzed quantitatively using frame grabbing equipment and image analysis software, as described in Chapter 3. Frames were individually examined, transverse flame displacements were measured, and lateral velocities were inferred from the known frame rate.

A planar CH_4/O_2 diffusion flame was subjected to Lorentz mixing under the influence of various magnetic field strengths. The video recording that was made during the experiment was viewed during slow-speed replay at rates of 30 and 4 frames per second (17 and 125 times slower than the actual experiment, respectively). Individual frames were also analyzed sequentially at each of seven magnetic flux densities.

With no magnetic field applied, a stable wedge of luminous gases rose vertically above the burner slot. A discharge was established across the flame and the area near burner exit became brighter. The shape of the product zone remained vertical. When a small magnetic field was applied, the flame began to oscillate left and right at the frequency of the driving a.c. current and the onset of a sinusoidal pattern could be seen. Figure 6.2 is a typical image showing the luminous product gases in the reaction zone. A complete cycle of the sine wave can be seen in the products above the burner exit. In Figure 6.3, the outline of the flame shape has been represented with line drawings to show a time sequence of the flame behavior in a low (0.016 T) magnetic field. The sequence represents one complete oscillation, or 1/60 s. The elapsed time between the images shown in Figure 6.3 is 0.004 s.

As the voltage across the electromagnet was increased the amplitude of the transverse oscillations (and thus the lateral velocity of the luminous region) also increased. When the magnetic flux density was further increased, the flow field was violently disrupted as the flame front was thrown far beyond the burner exit slots. The flame began to

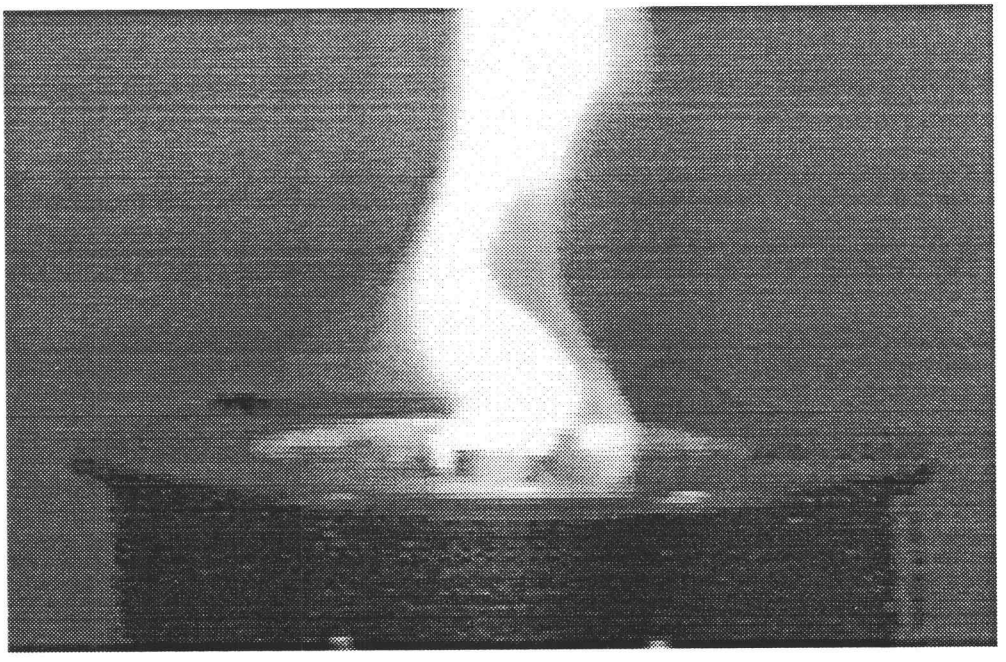

Figure 6.2 A Typical Oscillating Flame

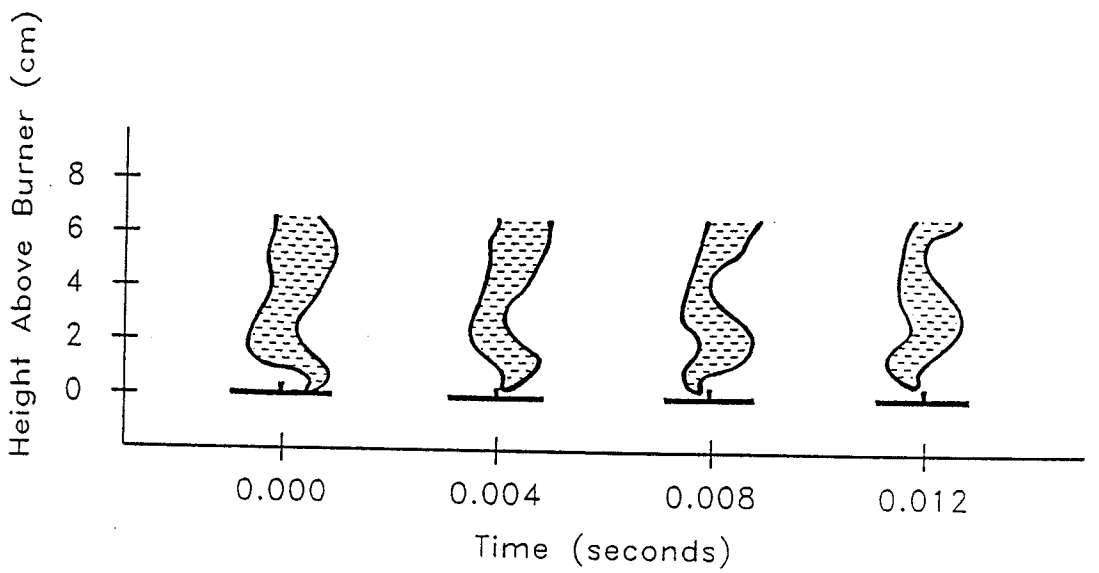

Figure 6.3 Flame Sequence at Low Magnetic Field

curl back upon itself and was sometimes broken apart into separate reaction regions. Figure 6.4 represents a time sequence of the flame behavior in a high (0.032 T) magnetic field. Again, the sequence represents one complete oscillation and the elapsed time between the images is 0.004 s. In Figure 6.5, typical images at four different field strengths are shown to indicate the increase in lateral amplitude as magnetic flux density increases.

Numerous series of video frames, representing the flame behavior at a variety of magnetic flux densities, were analyzed to determine maximum lateral gas velocities. The lateral flame velocity will track the waveform of the current, reaching a maximum magnitude twice per cycle. Velocity was inferred from the lateral distance moved between two successive frames. The elapsed time between frames was 0.002 s; the driving frequency of the flame (60 Hz) corresponds to 0.0167 s per flame oscillation. It therefore takes 8-1/3 video frames to capture a complete cycle of the flame, and the video frames will not always be aligned with maximum current events. The flame motion between two successive frames can therefore only be expected to accurately capture the maximum lateral velocity every third flame cycle. This misalignment is represented graphically in Figure 6.6. It was therefore important to examine three successive flame cycles and use the largest measured velocity as the most accurate representation of the true value. The distance traveled by the flame front between two well-chosen successive frames will then give a reasonable estimate of the maximum lateral velocity of the flame, subject to the considerations discussed in the next section.

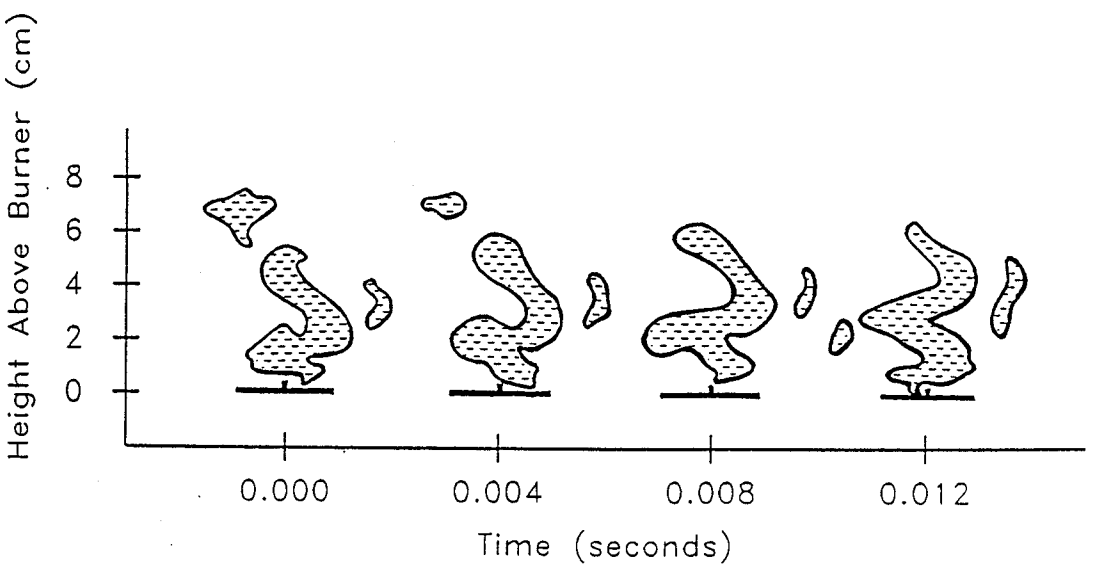

Figure 6.4 Flame Sequence at High Magnetic Field

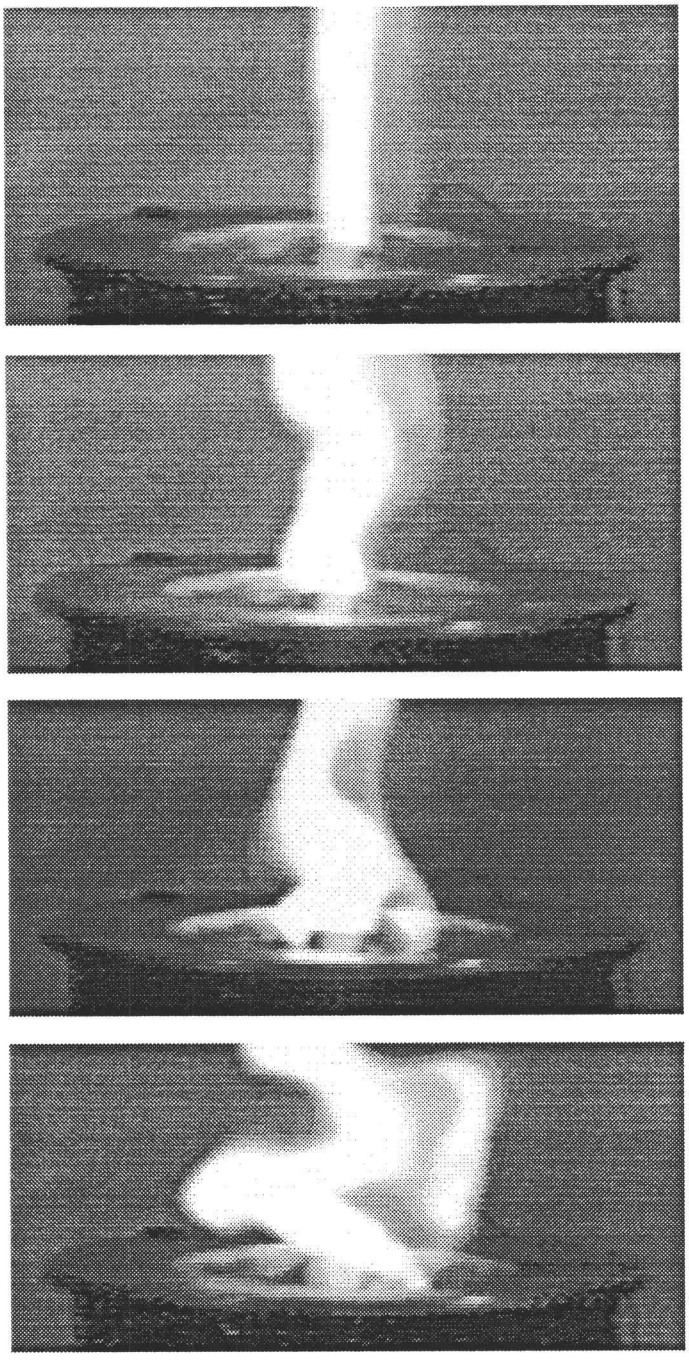

Figure 6.5 Four Flames at Increasing Magnetic Fields (a) No Field; (b) 80 gauss; (c) 160 gauss; (d) 320 gauss

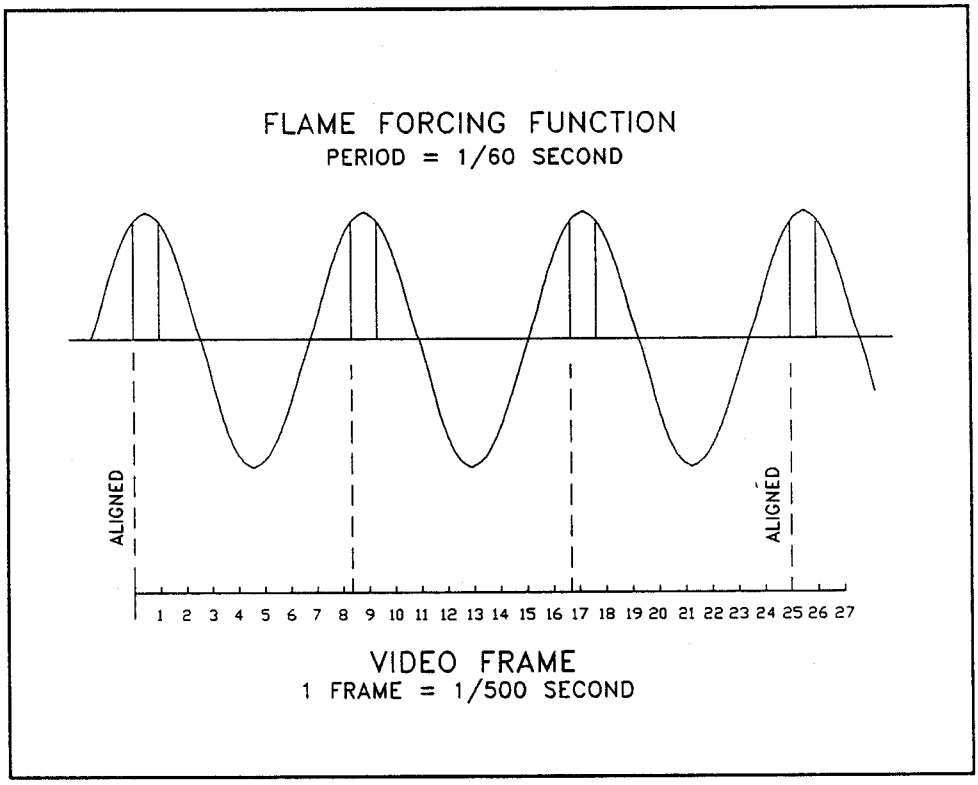

Figure 6.6 Misalignment of Video Frames with Flame Events

Figure 6.7 shows the experimental lateral velocities at seven different magnetic flux densities, calculated from video image analysis. Also plotted in the figure are the theoretical velocity curves described by equation (6.8) for three different values of the parameter η, which is a function of the peak current, drag coefficient, air density, and current path height. For the experimental data the peak current was 1.3 A. A drag coefficient of 1 is used, corresponding to that for an impermeable sheet. Taking the air density at 1000 K gives a value of 0.353 kg/m^3. The height of the current path is not precisely known but is estimated to be 0.008 m, giving η of approximately 30. The experimental data agree well with the trend predicted from theory and fall near the center curve, where η = 30.

6.4 Error Analysis

Using the method of Kline and McClintock (1953), the uncertainty in the calculated value η can be estimated for the experimental conditions. The values used in the calculation and their estimated uncertainties are i_{peak} = 1.3 $\pm$ 0.1 A; ρ^* = 0.353 $\pm$ 0.060 kg/m^3; b = 0.008 $\pm$ 0.002 m; and C_D = 1.0 $\pm$ 0.2. Most of the uncertainty in η comes from the inability to measure the height of the current path (b), and from the simplification that the drag coefficient (C_D) is that of an impermeable sheet. The resulting uncertainty in the calculated η is approximately 18%, so the calculated value is expected to lie in the range 25 to 36.

Error is introduced into the measurements of the video images in three ways. The first stems from the fact that distances are measured during image analysis using a calibrated caliper tool on the screen.

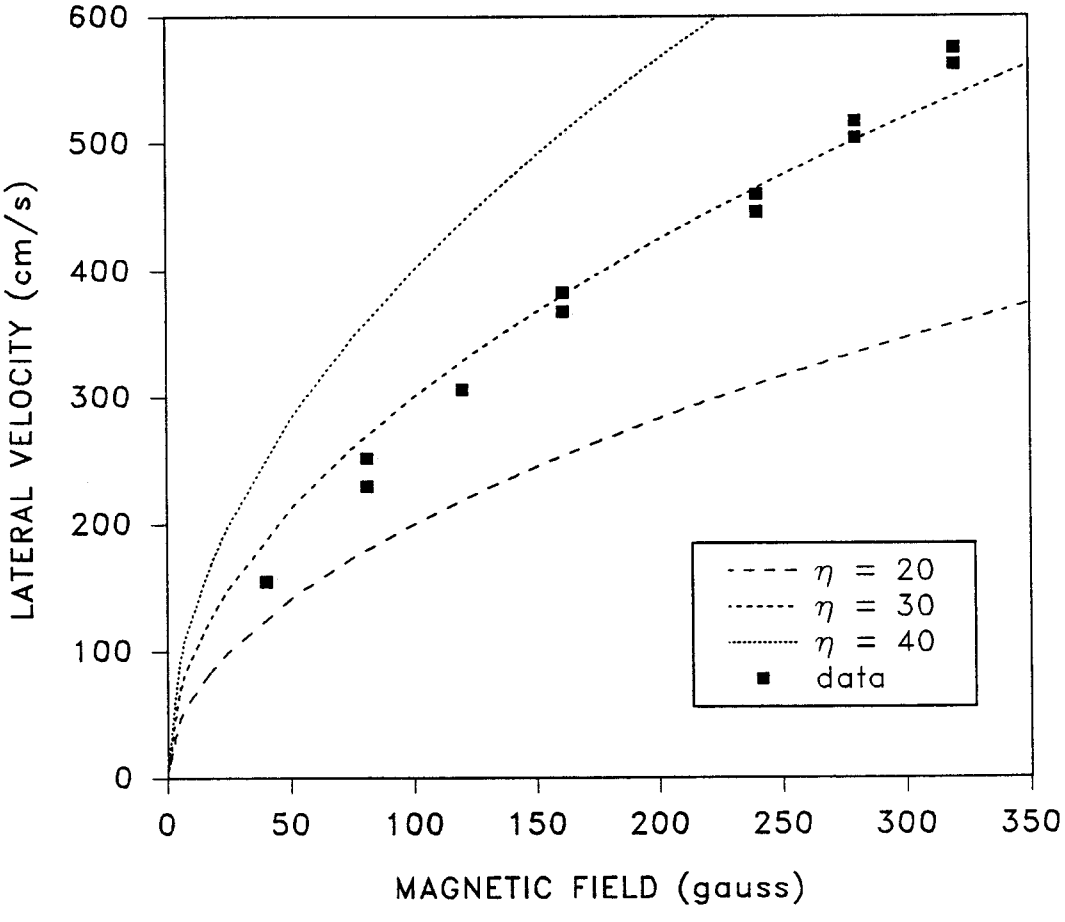

Figure 6.7 Experimental and Theoretical Lateral Velocities

The distance has error introduced because the flame edge is not precisely defined, making the caliper location subjective. Repeated measurements on the same image gave distances with repeatability within about 3%, which is small relative to other uncertainties.

The second source of error in the image analysis comes from the assumption that the maximum flame velocity can be accurately captured by viewing two well-chosen sequential frames. The time interval between frames is 0.002 s. If this were to capture an interval perfectly centered about the peak of the a.c. current, the average current could be found from:

$$i_{ave} = \frac{\int_{-0.001}^{0.001} i_{peak}[\cos(120\pi t)]\,dt}{\int_{-0.001}^{0.001} dt} \tag{6.9}$$

The average current would thus be 2.4% lower than the true maximum, resulting in a velocity measured in the video that would be 1.2% below the instantaneous maximum. This effect is negligible compared to the uncertainty due to other considerations.

The third consideration in the video image measurements relates to the assumed synchronization of the video frames with the a.c. driving force. As discussed in the previous section and described by Figure 6.6, every third cycle gives a higher velocity and is considered to coincide with the voltage peak. In the worst case, the highest velocity cycle could be displaced from the maximum by 1/6 of a frame, or 3.33×10^{-4} s. If the integration limits on equation (6.9) are changed accordingly, the average current during one frame will be 3.1% below the

peak value. This results in a measured velocity 1.6% below the instantaneous value, which is still negligible compared to the uncertainty from other sources.

The final consideration in the error analysis is the uncertainty in the magnetic flux density. As shown in Figure 3.7, the field was quite linear with applied coil voltage. The coil voltage was measured with an estimated uncertainty of $\pm$3%. When this is considered together with the uncertainty in the estimate of the height above the coil, the resulting uncertainty in the flux density is $\pm$6%.

6.5 Conclusions

A method has been investigated for mixing co-flowing reactant streams without physically invading the flow field. Properly oriented electric and magnetic fields are applied, resulting in an induced body force which can be used to manipulate a diffusion flame sheet. Induced lateral velocities have been observed which compare well with theoretical predictions. Lateral velocities of magnitudes large enough to induce bulk mixing were easily obtained, indicating that the method could potentially be applied for enhanced mixing in high-speed flows with shorter residence times.

7. SUMMARY

The effects of seeding a flame with trace quantities of an alkali element have been explored. The addition of a seed alters the flame's optical and electrical properties because alkalis have a lone electron in their outermost shell. They have strong emission spectra and ionize readily, thereby altering the properties of the entire flame although they comprise only a small fraction of its volume.

The emission characteristics of alkali-seeded flames make them amenable to optical temperature measurement techniques. A new method for measuring flame temperatures has been developed based on these principles. By monitoring the two resonance lines of the alkali element and subjecting each to different optical filtering, flame temperature can be inferred. The primary advantage of the new technique over those previously described is that it does not require adjustment of the background comparison radiation source. Other methods that have previously been reported which also share this advantage lack in temporal resolution. This is not a concern with the new method presented here.

One drawback of even the new method is that it cannot presently capture transient phenomena of very short duration. This is primarily an equipment limitation of the spectrographic instruments currently in use. Because the individual channels of the detector are scanned serially over a period of 0.015 ms, the two peaks being analyzed are recorded at slightly different times. This problem could be alleviated by using a detector which scans the channels in parallel. Also, the current detector loses sensitivity rapidly at the higher wavelength being monitored. This necessitates time averaging of about 100 scans to

sufficiently increase the signal to noise ratio. If a detector which was more sensitive in the near infrared region were used, the need to time average could potentially be eliminated. Another possible scenario involves time averaging of a gated signal which has been synchronized to the period of the oscillating event being captured.

The addition of alkali seed to a flame also increases its electrical conductivity by several orders of magnitude. This allows a current to be passed through a flame at normal flame temperatures. The current carrying properties of planar diffusion flames have been studied and found to compare in many ways with those previously reported for premixed flames. Characterization of the electrical properties of diffusion flames was necessary for the work carried out here, but should also prove useful for related work in the field.

It has also been shown that electric and magnetic fields can be used to manipulate a diffusion flame and enhance mixing. Both theoretical considerations and experimental results support the feasibility of this process. A planar flame was subjected to induced Lorentz forces which were oscillated to enhance bulk mixing of the reactants. The magnitude of the forces developed was sufficient to greatly disrupt the laminar flow field.

The enhancement of bulk mixing was verified visually from high-speed video images. In the future it would also be interesting to explore the mixing effect more quantitatively, for example with measurements of temperature and/or species concentrations throughout the flame region. The high frequency of the transient events would require exploring some of the previously discussed changes to the temperature measurement technique.

The real interest in a method which enhances mixing is for high-speed flows. The next logical step in pursuing this technique would involve both theoretical and experimental work with higher speed flames than those studied here, to determine whether similar enhancement can be achieved. It would be interesting to generate a complete transient numerical model of the low-speed flow system, using the experimental results to verify the numerical model. Higher speed flames could then be modeled numerically to explore the possible effectiveness of subjecting them to Lorentz-enhanced mixing. If the prospects looked promising, the numerical model could also be used for experimental planning and design prior to construction of a higher speed facility.

8. BIBLIOGRAPHY

Altenkirch, R.A., Peck, R.E., and Chen, S.L., 1979, "The Appearance of Nitric Oxide and Cyanide in One-Dimensional Coal Dust/Oxidizer Flames," *Combustion Science and Technology*, Vol. 20, pp. 49-58.

Angrist, S.W., 1982, Direct Energy Conversion, 4th ed., Allyn & Bacon, Boston, pp. 279-289.

Bussing, T.R.A. and Eberhardt, S., 1989, "Chemistry Associated with Hypersonic Vehicles," *J. Thermophysics*, Vol. 3, pp. 245-253.

Chen, D.C.C., Lawton, J., and Weinberg, F.J., 1965, "Augmenting Flames With Electric Discharges," *10th Symposium (International) on Combustion*, The Combustion Institute, pp. 743-754.

Crawford, R.A., Chapman, J.N., and Rhodes, R.P., 1990, "Performance Potential and Technology Issues of MHD Augmented Hypersonic Simulation Facilities," *AIAA 16th Aerodynamic Ground Testing Conference, Paper #90-1380*, Seattle WA, June 18-20, pp. 1-9.

Cussler, E.L., 1984, Diffusion Mass Transfer in Fluid Systems, Cambridge University Press, pp. 105-113.

Daily, J.W. and Kruger, C.H., 1976, "Boundary Layer Measurements of Temperature and Electron Number Density Profiles in a Combustion MHD Generator," Combustion Measurements--Modern Techniques and Instrumentation (R. Goulard, editor), Academic Press, New York, pp. 119-126.

Davies, R.M., 1965, "Heat Transfer Measurements on Electrically Boosted Flames," *10th Symposium (International) on Combustion*, The Combustion Institute, pp. 755-766.

De Vos, J.C., 1954, "A New Determination of the Emissivity of Tungsten Ribbon," *Physica*, Vol. 20, pp. 690-714.

Dimmock, T.H. and Kineyko, W.R., 1963, "The Low Pressure, Combustion Gas Plasma," *Combustion and Flame*, Vol. 7, pp. 283-291.

Fells, I., Gawen, J.C., and Harker, J.H., 1967, "An Investigation into the Electrical Conductivities of Propane-Air Flames Augmented with D.C. Electrical Power," *Combustion and Flame*, Vol. 11, pp. 309-319.

Fristrom, R.M. and Westenberg, A.A., 1965, Flame Structure, McGraw-Hill, New York, pp. 150-152.

Gaydon, A.G., 1974, The Spectroscopy of Flames, 2nd ed., Chapman and Hall Ltd., London, pp. 65-66.

Gaydon, A.G. and Wolfhard, H.G., 1970, Flames - Their Structure, Radiation, and Temperature, 3rd ed., Chapman and Hall Ltd., London, pp. 239-270.

Halliday, D. and Resnick, R., 1967, Physics Part II, Wiley, New York, pp. 818-819.

Haynes, B.S., Jander, H., and Wagner, H.G., 1978, "The Effect of Metal Additives on the Formation of Soot in Premixed Flames," *17th Symposium (International) on Combustion*, The Combustion Institute, pp. 1365-1374.

Karlovitz, B., 1962, "Flames Augmented by Electrical Power," *Pure and Applied Chemistry*, Vol. 5, pp. 557-566.

Katz, J.L. and Hung, C-H., 1990, "Initial Studies of Electric Field Effects on Ceramic Powder Formation in Flames," *23rd Symposium (International) on Combustion*, The Combustion Institute, pp. 1733-1738.

Kimura, I. and Ogiwara, K., 1974, "Application of Magnetic Field to Flames Augmented by High-Voltage Discharge," *15th Symposium (International) on Combustion*, The Combustion Institute, pp. 1031-1036.

Kline, S.J. and McClintock, F.A., 1953, "Describing Uncertainties in Single-Sample Experiments," *Mechanical Engineering*, Jan. 1953, pp. 3-8.

Klingenberg, G. and Mach, H., 1976, "Investigation of Combustion Phenomena Associated with the Flow of Hot Propellant Gases - Spectroscopic Temperature Measurements Inside the Muzzle Flash of a Rifle," *Combustion and Flame*, Vol. 27, pp. 163-176.

Kuhn, H.G., 1969, Atomic Spectra, 2nd ed., Academic Press, pp. 151-175.

Kurlbaum, F., 1902a, "Über Eine Einfache Methode, die Temperatur Leuchtender Flammen zu Bestimmen," *Physikalische Zeitschrift*, Vol. 3, pp. 187-188.

Kurlbaum, F., 1902b, "Über das Reflexionsvermögen von Flammen," *Physikalische Zeitschrift*, Vol. 3, pp. 332-334.

Lapp, M. and Hartley, D.L., 1976, "Raman Scattering Studies of Combustion," Combustion Measurements--Modern Techniques and Instrumentation (R. Goulard, editor), Academic Press, New York, pp. 135-156.

Lapp, M. and Rich, J.A., 1963, "Electrical Conductivities of Seeded Flame Plasmas in Strong Electric Fields," *Phys. Fluids*, Vol. 6, pp. 806-816.

Malmstadt, H.V., Enke, C.G., and Crouch, S.R., 1981, Electronics and Instrumentation for Scientists, Benjamin/Cummings, Menlo Park, CA, pp. 86-87.

Mitani, T. and Niioka, T., 1984, "Extinction Phenomenon of Premixed Flames with Alkali Metal Compounds," *Combustion and Flame*, Vol. 55, pp. 13-21.

Nakamura, J., 1959, "Effect of the Electric Field upon the Spectra of the Hydrocarbon Diffusion Flame," *Combustion and Flame*, Vol. 3, pp. 277-284.

Newman, R.M. and Page, F.M., 1973, "The Dispersion of Spray Droplets in Flames," *Combustion and Flame*, Vol. 20, pp. 171-176.

Penner, S.S., 1949, "Optical Methods for the Determination of Flame Temperatures I. Two-Color and Line-Reversal Techniques," *American Journal of Physics*, Vol. 17, pp. 422-429.

Place, E.R. and Weinberg, F.J., 1965, "Electrical Control of Flame Carbon," *Proceedings of the Royal Society*, Vol. A289, pp. 192-205.

Reif, I., Fassel, V.A., and Kniseley, R.N., 1973, "Spectroscopic Flame Temperature Measurements and their Physical Significance - I. Theoretical Concepts - A Critical Review," *Spectrochimica Acta*, Vol. 28B, pp. 105-123.

Siegel, R. and Howell, J.R., 1981, Thermal Radiation Heat Transfer, 2nd ed., McGraw-Hill, New York, pp. 18-23.

Strong, H.M. and Bundy, F.P., 1954a, "Measurement of Temperatures in Flames of Complex Structure by Resonance Line Radiation. I. General Theory and Application to Sodium Line Reversal Methods," *Journal of Applied Physics*, Vol. 25, pp. 1521-1526.

Strong, H.M. and Bundy, F.P., 1954b, "Measurement of Temperatures in Flames of Complex Structure by Resonance Line Radiation. II. Sodium Line Reversal by High-Resolution Spectroscopy," *Journal of Applied Physics*, Vol. 25, pp. 1527-1530.

Strong, H.M. and Bundy, F.P., 1954c, "Measurement of Temperatures in Flames of Complex Structure by Resonance Line Radiation. III. From Absolute Intensity Measurements at High Resolution," *Journal of Applied Physics*, Vol. 25, pp. 1521-1526.

Thomas, D.L., 1968a, "Problems in Applying the Line Reversal Method of Temperature Measurement to Flames," *Combustion and Flame*, Vol. 12, pp. 541-549.

Thomas, D.L., 1968b, "An Automatic Remotely Operated Sodium D-Line Reversal Temperature Measuring Technique," *Combustion and Flame*, Vol. 12, pp. 569-574.

Uhlherr, M.B. and Walsh, B.W., 1971, "DC Discharges in Seeded Propane-Air Flames," *Combustion and Flame*, Vol. 17, pp. 45-54.

Weast, R.C. (editor), 1973, Handbook of Chemistry and Physics, 53rd ed., The Chemical Rubber Company, Cleveland, pp. E198-E201.

Weinberg, F.J., 1986, Advanced Combustion Methods, Academic Press, London, pp. 280-289.

Wolfhard, H.G. and Parker, W.G., 1949, "A New Technique for the Spectroscopic Examination of Flames at Normal Pressures," *Proceedings of the Physics Society*, Vol. A62, pp. 722-730.

APPENDICES

APPENDIX A

NOMENCLATURE

a_{lat} = lateral acceleration

A_p = area perpendicular to direction of motion

A_{slot} = area of fuel slot of diffusion burner

b = height of current carrying region of gas

B = magnetic flux density

C = second radiation constant = 0.014388 m-K

C_D = drag coefficient of flame sheet

C_P = heat capacity of gas

d_{bead} = diameter of thermocouple bead

D_{CH4} = diffusion coefficient of methane into flame zone

$f_{Lorentz}$ = Lorentz body force per unit volume

F_{drag} = drag force on moving flame sheet

$F_{Lorentz}$ = Lorentz body force

i = current through flame

I = radiation intensity

j = current density through flame

k = thermal conductivity of gas

l = length of optical path through flame; length of current path through flame

$\dot{m}$ = mass flowrate

$\dot{m}_{CH4}$ = burner mass flowrate of methane

$\dot{m}_{diff}$ = diffusion mass flowrate into reaction zone

$\dot{Q}$ = heat flux

R = ratio of peak heights at λ_1 and λ_2

s = thickness of current carrying region of gas

t = time

$t_{\lambda 1}$ = net transmission through color filter and first lens at lower transition wavelength

T = temperature

u = inlet velocity

v_{lat} = lateral flame sheet velocity

V = voltage across flame; volume of gas

w_{Tb} = uncertainty in brightness temperature

w_{Tfil} = uncertainty in filament temperature

x = measure of position in flame

Greek

α = absorption coefficient of gas

ΔI = peak height above background spectrum

ΔT = temperature difference

ϵ = emissivity of thermocouple bead

$\epsilon_{\lambda,Tfil}$ = emissivity of filament at a given wavelength and temperature

λ = wavelength

η = proportionality constant in velocity/magnetic field relation (defined on page 76)

ρ = density

σ = Stefan-Boltzman constant = 5.67×10^{-8} W/m^2-K^4

ϕ = stoichiometric equivalence ratio of flame

Subscripts

ave = average value during a given time interval of a.c. cycle

b = brightness temperature of radiation source (lamp)

$CH4$ = referring to flowrate of methane only

$cond$ = conduction

$conv$ = convection

d = with discharge through flame

f = flame

fil = filament temperature of radiation source (lamp)

$peak$ = maximum value during a.c. cycle

rad = radiation

tc = thermocouple

1 = lower transition wavelength of alkali doublet; lower position in diffusion flame

2 = upper transition wavelength of alkali doublet; upper position in diffusion flame

∞ = ambient

Superscripts

* = measured at temperature just outside flame

o = measured at standard conditions

APPENDIX B

ASYST DATA ACQUISITION PROGRAM

```
\ ************************************************************************
\
\          Signal Averaging Routine for Spectrometer
\
\ This program allows ASYST to Interface to EG&G PARC
\ Spectrometer Model 1461 with GPIB address 12.
\ It produces a continuously averaged scan of the spectrometer
\ output and displays it graphically.  The user inputs the number
\ of scans to be averaged.  The program also can be used for
\ directly sending 1461 commands or for performing ASYST
\ commands.
\
\ Written by:  Heidi Pattee
\ Last update: October 3, 1991
\
\ Requirements:  ASYST version 1.53 or greater
\                ASYST module 4
\                IBM PC\XT\AT or compatible
\                GPIB Interface Board compatible with ASYST
\                        (see ASYST documentation for list)
\
\ Note:  ASYST must be properly configured for the intended GPIB
\        board before loading this program.  The GPIB board and
\        its handler software must also be properly installed on
\        the host system.
\
\ Directions:
\        1.  Load this program.  Then type "GO" to start it.
\        2.  Make sure you are in CAPS LOCK mode.
\
\ Acknowledgement:  ASYST is a trademark of Macmillan Software Co.
\
\ ************************************************************************
\
\
\
\       VARIABLE DECLARATIONS
\
INTEGER SCALAR S.POLL                   \ SERIAL POLL RESPONSE
INTEGER DIM[ 8 ] ARRAY S.POLL.BIT       \ ARRAY OF S.POLL BITS
75 STRING CMD.OUT
75 STRING RESPONSE
```

```
REAL DIM[ 513 ] ARRAY DATA
REAL DIM[ 513 ] ARRAY BACKGROUND      \ BACKGROUND SCAN FOR SUBTRACTION
REAL DIM[ 513 ] ARRAY DATASM          \ SMOOTHED CURVE (FOR PK HEIGHTS)
REAL SCALAR RATIO                     \ PEAK HEIGHT RATIO
INTEGER SCALAR N
INTEGER SCALAR M
INTEGER DIM[ 25000 ] ARRAY BUFF.ARRAY
INTEGER SCALAR RSP.CTR
INTEGER SCALAR OLD.CTR
INTEGER SCALAR REPEATS
INTEGER SCALAR SUBTRACT.FLAG
REAL SCALAR TB1 REAL SCALAR T.A REAL SCALAR R.A
REAL SCALAR TB2 REAL SCALAR T.B REAL SCALAR R.B
REAL SCALAR T.MID REAL SCALAR R.MID REAL SCALAR C2
REAL SCALAR LAMBDA1
REAL SCALAR LAMBDA2
INTEGER SCALAR TFLAME
1 STRING CMP.CHR                      \ CHARACTER USED TO
" `" CMP.CHR ":=                      \ PREFIX ASYST WORDS
\
: INIT.PGM                            \ SET UP SPECTROMETER PARAMETERS
    NORMAL.DISPLAY
    STACK.CLEAR
    8 3 FIX.FORMAT
    12 " GPIB.DEVICE DEV1" "EXEC
    10000 TIMEOUT
    SEND.INTERFACE.CLEAR
    REMOTE.ENABLE.ON
    13 EOS.CHARACTER                   \ USE CR AS EOS
    EOS.ON
    " DD 13;DA 4;ET .015"              \ USE CR AS DELIMITER
    CMD.OUT ":=                        \ SET UP D.A. MODE 4.  SET
    0 DATA :=                          \ EXPOSURE TIME TO 0.015 SEC.
    0 BACKGROUND :=
    0 SUBTRACT.FLAG :=
    1 REPEATS :=
    0 TB1 := 0 TB2 := 852E-9 LAMBDA1 := 894E-9 LAMBDA2 :=
    0.014388 C2 :=
;
: HELP                                \ HELP MENU SCREEN
    CR
    CR
    ."    ************************************************************" CR
    ."    |       TYPE ANY 1461 COMMAND                              |" CR
    ."    |  OR   TYPE ANY ASYST COMMAND PRECEDED BY `               |" CR
    ."    |                                                          |" CR
    ."    |       FUNCTION KEYS:                                     |" CR
    ."    |                                                          |" CR
    ."    |       F3  RETURN TO ASYST                                |" CR
    ."    |       F4  TAKE A NEW BACKGROUND SIGNAL READING           |" CR
    ."    |       F5  SIGNAL AVG WITH BACKGROUND SUBTRACTION         |" CR
    ."    |       F6  SIGNAL AVG WITHOUT BACKGROUND SUBTRACTION      |" CR
    ."    |       F7  CAPTURE CURRENT CURVE INTO DATA FILE           |" CR
    ."    | SHIFT-F7  GET PEAK HEIGHT RATIO FROM LAST SCAN           |" CR
```

```
    ."     ¦  CTRL-F7  DEFINE RAD. SOURCE BRIGHTNESS TEMPERATURES ¦" CR
    ."     ¦   ALT-F7  CALCULATE FLAME TEMPERATURE                ¦" CR
    ."     ************************************************************" CR
;
: GET.CMD
    HELP
    CR ." ENTER COMMAND: "
    "INPUT
    CMD.OUT ":=
;
: INT.CMD                                   \ INTERPRET CMD FOR ASYST WORD
    CMP.CHR                                 \ OR DEVICE COMMAND
    CMD.OUT
    1 "LEFT
    "=
    IF                                      \ IF IT STARTS WITH ` IT IS AN
        CMD.OUT "LEN 1 -                    \ ASYST COMMAND.  REMOVE THE `
        "RIGHT                              \ AND SET "TRUE"
        CMD.OUT ":=
        TRUE
    ELSE                                    \ OTHERWISE IT IS A DEVICE
        FALSE                               \ COMMAND SO SET "FALSE"
    THEN
;
: SER.POL
    255 SERIAL.POLL
    DUP S.POLL :=
    #>MASK
    ?DUP 128, AND MASK>#  S.POLL.BIT [ 8 ] :=
    ?DUP 64, AND MASK>#  S.POLL.BIT [ 7 ] :=
    ?DUP 32, AND MASK>#  S.POLL.BIT [ 6 ] :=
    ?DUP 16, AND MASK>#  S.POLL.BIT [ 5 ] :=
    ?DUP 8, AND MASK>#  S.POLL.BIT [ 4 ] :=
    ?DUP 4, AND MASK>#  S.POLL.BIT [ 3 ] :=
    ?DUP 2, AND MASK>#  S.POLL.BIT [ 2 ] :=
    1, AND MASK>#  S.POLL.BIT [ 1 ] :=
;
: SEND.CMD
    BEGIN
        SER.POL
        S.POLL.BIT [ 1 ] #>MASK         \ WAIT FOR PRE CMD DONE
    UNTIL
    GPIB.WRITE
;
: GET.RSP
    RSP.CTR OLD.CTR :=
    0 RSP.CTR :=
    BEGIN
        SER.POL
        S.POLL.BIT [ 8 ] #>MASK         \ OUTPUT READY?
        IF
            1 RSP.CTR + RSP.CTR :=
            RESPONSE GPIB.READ
            13 RESPONSE
```

```
            "NUMBER                         \ CONVERT RESPONSE TO A NUMBER
            DATA [ RSP.CTR ] :=             \ AND STORE IN "DATA" ARRAY
            IF NOP THEN                     \ THROW OUT A LOGICAL VALUE
            "DROP                           \ THROW OUT AFTER STRING
        THEN
        S.POLL.BIT [ 1 ] #>MASK             \ CMD DONE?
    UNTIL
;
: PRINT.RSP
    S.POLL.BIT [ 2 ] #>MASK
    IF
        BELL
        CR
        ." COMMAND ERROR" CR
        OLD.CTR RSP.CTR :=                  \ RESTORE OLD COUNTER
    ELSE
        RSP.CTR 0 =
        IF
            CR
        ELSE
            DATA SUB[ 1 , RSP.CTR , 1 ] .
            CR
        THEN
    THEN
;
: COMPLETE.SEND
    SEND.CMD
    GET.RSP
    PRINT.RSP
;
: CHECK.KEYS
    STACK.RESET
    ?KEY
    IF
        PCKEY
        IF
            INTERPRET.KEY
        THEN
    THEN
;
: MAIN.PGM
    BEGIN
        STACK.RESET
        NORMAL.DISPLAY
        GET.CMD
        INT.CMD
        IF                                  \ SEND ASYST COMMAND
            CMD.OUT
            "EXEC
            CR
        ELSE                                \ SEND DEVICE COMMAND
            CMD.OUT
            COMPLETE.SEND
        THEN
```

```
        CR ."    *** HIT ANY KEY TO CONTINUE ***" CR
        KEY DROP
        CHECK.KEYS
    AGAIN
    ONESCAPE: MYSELF
    ONERR: BELL
    CR ." ERROR DETECTED. HIT ANY KEY TO CONTINUE " CR
    KEY DROP
    MYSELF
;
: GO
    INIT.PGM
    CMD.OUT SEND.CMD
    MAIN.PGM
;
: SETUP.GRAPH
    GRAPHICS.DISPLAY
    HORIZONTAL GRID.OFF
    VERTICAL GRID.OFF
    HORIZONTAL AXIS.FIT.OFF
    0 512 HORIZONTAL WORLD.SET
    0 0 VUPORT.ORIG
    1 1 VUPORT.SIZE
    8 10 AXIS.DIVISIONS
    2 2 HORIZONTAL LABEL.POINTS
    1 2 VERTICAL LABEL.POINTS
    VUPORT.CLEAR
    OUTLINE
    XY.AXIS.PLOT
    NORMAL.COORDS
    .400 .02 POSITION " Hit F10 to Exit" LABEL
    .400 .05 POSITION " Hit F9 to Manual Scale" LABEL
    .400 .08 POSITION " Hit F8 to Autoscale" LABEL
    WORLD.COORDS
    BUFF.ARRAY LINE.BUFFER.ON
;
: ACTUAL.SCAN
    STACK.RESET
    BEGIN
        " RUN;DC 1,1,512"                \ SEND SCAN COMMAND TO
        SEND.CMD                         \ SPECTROMETER
        GET.RSP
        DATA REPEATS /
        SUBTRACT.FLAG 1 = IF
            BACKGROUND -
        THEN
        DATA :=
        CHECK.KEYS
        ERASE.LINES
        DATA SUB[ 4 , 509 , 1 ] Y.DATA.PLOT
    AGAIN
;
: SCAN.START
    " I " REPEATS "." "CAT
```

```
    COMPLETE.SEND
    0 4000 VERTICAL WORLD.SET
    SETUP.GRAPH
    ACTUAL.SCAN
;
: SCAN
    CR
    ." ENTER THE NUMBER OF SCANS TO BE AVERAGED "
    "INPUT
    32 "NUMBER REPEATS :=
    SCAN.START
;
: RETURN.TO.ASYST                    \ FUNCTION FOR F3 KEY
    QUIT
;
: GET.BACKGROUND                     \ FUNCTION FOR F4 KEY
    CR CR ." ***PLEASE WAIT*** "
    " I " 100 "." "CAT
    COMPLETE.SEND
    " RUN;DC 1,1,512"
    SEND.CMD
    GET.RSP
    DATA 100 / BACKGROUND :=
    ESCAPE
;
: SUBTRACT.BACKGROUND                \ FUNCTION FOR F5 KEY
    1 SUBTRACT.FLAG :=
    SCAN
;
: DONT.SUBTRACT.BACKGROUND           \ FUNCTION FOR F6 KEY
    0 SUBTRACT.FLAG :=
    SCAN
;
: CAPTURE                            \ FUNCTION FOR F7 KEY
    FILE.TEMPLATE DATA []FORM.SUBFILE END
    CR ." ENTER THE FILENAME "
    "INPUT
    "DUP DEFER> FILE.CREATE
    DEFER> FILE.OPEN
    DATA ARRAY>FILE
    FILE.CLOSE
    ESCAPE
;
: RATIO.CALC
    .05 SET.CUTOFF.FREQ
    DATA DATA SMOOTH SMOOTH SMOOTH - DATASM :=   \ STORE PK HT ABOVE
    61 N :=                                      \ CURVE IN DATASM
    70 53 DO
        DATASM [ I ] ABS DATASM [ N ] ABS >
        IF I N := THEN
    LOOP                        \ FIND LOCATION OF 1ST PEAK; STORE IN N
    426 M :=
    435 418 DO
        DATASM [ I ] ABS DATASM [ M ] ABS >
```

```
      IF I M := THEN          \ FIND LOCATION OF 2ND PEAK; STORE IN M
    LOOP
    DATA SMOOTH DATASM :=           \ PUT BASELINE CURVE IN DATASM
    DATA [ N ] DATASM [ N 36 - ] DATASM [ N 36 + ] + 2 / -
    DATA [ M ] DATASM [ M 36 - ] DATASM [ M 36 + ] + 2 /
         - / 15 / RATIO :=     \ GET RATIO OF PEAK HEIGHTS ABOVE AVG
                               \ BASELINE SIGNAL (+/- 36 CHANNELS)
;
: GET.RATIO                    \ FUNCTION FOR SHIFT-F7 KEY
    CR ." CALCULATING RATIO--PLEASE WAIT..."
    RATIO.CALC
    CR CR ." THE PEAK HEIGHT RATIO IS " RATIO .
    CR CR ."   *** HIT ANY KEY TO CONTINUE ***" CR
    KEY DROP ESCAPE
;
: SOURCE.TEMPS
    CR ." ENTER BRIGHTNESS TEMPERATURE AT 852 nm " #INPUT TB1 :=
    CR ." ENTER BRIGHTNESS TEMPERATURE AT 894 nm " #INPUT TB2 :=
;
: REDO.SOURCE.TEMPS            \ FUNCTION FOR CTRL-F7 KEY
    SOURCE.TEMPS
    ESCAPE
;
: RCALC                        \ THE "PATTEE EQUATION" FOR R VS T :-)
    DUP
    INV C2 * LAMBDA1 / NEG EXP C2 LAMBDA1 / TB1 / NEG EXP -
    C2 LAMBDA2 / ROT / NEG EXP C2 LAMBDA2 / TB2 / NEG EXP - /
    LAMBDA2 LAMBDA1 / 5 ** *
;
: CALCULATE.TEMP               \ FUNCTION FOR ALT-F7 KEY
    STACK.RESET
    TB1 0 <= TB2 0 <= OR       \ CALL SOURCE.TEMPS IF TB1 AND TB2
    IF SOURCE.TEMPS THEN       \ HAVEN'T BEEN PROPERLY DEFINED
    CR ." SCANNING FLAME 100 TIMES..."
    100 REPEATS :=
    " I " REPEATS "." "CAT
    COMPLETE.SEND
    " RUN;DC 1,1,512"          \ SEND SCAN COMMAND TO SPECTROMETER
    SEND.CMD
    GET.RSP
    DATA REPEATS /
    BACKGROUND -
    DATA :=
    CR ." CALCULATING FLAME TEMPERATURE..."
    RATIO.CALC
    TB1 300 - T.A :=
    TB2 300 + T.B :=
    T.A RCALC R.A :=
    T.B RCALC R.B :=
    RATIO R.A <                \ FIGURE OUT IF TEMP LIES ABOVE OR
    IF TB2 1 - T.B :=          \ BELOW TB2, BASED ON THE RATIO
    ELSE RATIO R.B >
      IF TB2 1 + T.A :=
      ELSE CR ." TEMPERATURE IS OUTSIDE THE RANGE "
```

```
        T.A . ." TO " T.B .
        CR ."  *** HIT ANY KEY TO CONTINUE *** " KEY DROP
        ESCAPE
      THEN
    THEN
    T.A RCALC RATIO - R.A :=
    T.B RCALC RATIO - R.B :=
    BEGIN
        T.A T.B + 2 / T.MID :=
        T.MID RCALC RATIO - R.MID :=
        R.A R.MID * 0 <
        IF R.MID R.B := T.MID T.B :=
        ELSE R.MID R.A := T.MID T.A :=
        THEN
    T.B T.A - 1 < UNTIL
    T.A T.B + 2 / TFLAME :=
    CR ." THE FLAME TEMPERATURE IS " TFLAME . ."  KELVIN"
    CR ."  *** HIT ANY KEY TO CONTINUE *** "  KEY DROP
    ESCAPE
;
: AUTO.SCALE                                  \ FUNCTION FOR F8 KEY
    BUFF.ARRAY LINE.BUFFER.OFF
    LINE.BUFFER.CLEAR
    VERTICAL AXIS.FIT.ON
    DATA []MIN DATA []MAX VERTICAL WORLD.SET
    SETUP.GRAPH
    DATA SUB[ 4 , 509 , 1 ] Y.DATA.PLOT
    ACTUAL.SCAN
;
: MANUAL.SCALE                                \ FUNCTION FOR F9 KEY
    BUFF.ARRAY LINE.BUFFER.OFF
    LINE.BUFFER.CLEAR
    VERTICAL AXIS.FIT.OFF
    NORMAL.DISPLAY
    CR ." ENTER LOWER LIMIT OF Y AXIS "
    #INPUT
    CR ." ENTER UPPER LIMIT OF Y AXIS "
    #INPUT
    VERTICAL WORLD.SET
    SETUP.GRAPH
    DATA SUB[ 4 , 509 , 1 ] Y.DATA.PLOT
    ACTUAL.SCAN
;
F3 FUNCTION.KEY.DOES RETURN.TO.ASYST
F4 FUNCTION.KEY.DOES GET.BACKGROUND
F5 FUNCTION.KEY.DOES SUBTRACT.BACKGROUND
F6 FUNCTION.KEY.DOES DONT.SUBTRACT.BACKGROUND
F7 FUNCTION.KEY.DOES CAPTURE
F7 SHIFT FUNCTION.KEY.DOES GET.RATIO
F7 CTRL FUNCTION.KEY.DOES REDO.SOURCE.TEMPS
F7 ALT FUNCTION.KEY.DOES CALCULATE.TEMP
F8 FUNCTION.KEY.DOES AUTO.SCALE
F9 FUNCTION.KEY.DOES MANUAL.SCALE
F10 FUNCTION.KEY.DOES ESCAPE
```